CHALMERS
UNIVERSITY OF TECHNOLOGY

Magnetic separation of oxygen carriers from bed ash in heat and power plants

Master's thesis in Applied Physics

Frida Karlsson

Department of Space, Earth and Environment
Chalmers University of Technology
Gothenburg, Sweden 2019

Master's thesis 2019

Magnetic separation of oxygen carriers from bed ash in heat and power plants

Frida Karlsson

CHALMERS
UNIVERSITY OF TECHNOLOGY

Department of Space, Earth and Environment
Division of Energy Technology
Chalmers University of Technology
Gothenburg, Sweden 2019

Magnetic separation of oxygen carriers from bed ash in heat and power plants
Frida Karlsson

Supervisor: Patrick Moldenhauer, Department of Space, Earth and Environment
Examiner: Tobias Mattisson, Department of Space, Earth and Environment

Master's Thesis 2019
Department of Space, Earth and Environment
Energy Technology
Chalmers University of Technology
SE-412 96 Gothenburg
Telephone +46 31 772 1000

Typeset in LaTeX
Gothenburg, Sweden 2019

Magnetic separation of oxygen carriers from bed ash in heat and power plants
FRIDA KARLSSON
Department of Space, Earth and Environment
Chalmers University of Technology

Abstract

In response to climate change, research is currently conducted on the possibility of reducing the CO_2 emissions from combustion plants. Technologies utilizing fluidized beds can be used for combustion with low emissions. Chemical-looping combustion (CLC) and oxygen carrier aided combustion (OCAC) are two such technologies, using fluidized beds with an oxygen-carrying bed material, which can be used instead of sand to transport oxygen between air and fuel. To minimize resource use and costs, it is important to reuse spent oxygen carriers. The possibility of recycling and reusing these oxygen carriers is studied in this work by separating the metal-based oxygen carriers from fuel ash through magnetic separation, and is based on the results of a previous Bachelor thesis project conducted in 2018.

In this thesis, the magnetic properties of three oxygen carrier materials, ilmenite, LS Slag and Sibelco Calcined, that have been used in combustion processes are investigated using different characterization techniques. This is done in order to obtain a better understanding of the mechanisms which govern the magnetic behavior of oxygen carrier materials. Of the investigated materials, ilmenite and LD Slag are iron-based and Sibelco Calcined is manganese-based. Correlations between data from magnetic separation of these materials obtained in the Bachelor thesis and data obtained in this project are investigated. Different experimental techniques were employed, including measurements of magnetic susceptibility, X-ray powder diffraction (XRD) and scanning electron microscopy (SEM) with energy dispersive X-ray spectroscopy (EDX). The possibility to create a model by which the magnetic fraction can be predicted is further explored.

The results indicate that there is some correlation between magnetic susceptibility and the obtained magnetic fraction, though not to the extent that would be needed in order to create a model. The results further suggest that the iron-oxide magnetite (Fe_3O_4), common in the iron-based oxygen carriers, is significant to the magnetic separability of these oxygen carrier materials. An oxygen carrier based on manganese ores could still be separated through magnetism, although this will likely depend upon the amount of iron in the sample. Suggestions can be made to use manganese ores with high concentrations of iron, as this is indicated to increase the magnetic properties of the material.

Keywords: Chemical-looping combustion, circulating fluidized bed, oxygen-carrier aided combustion, oxygen carrier, carbon capture and storage, ilmenite, LD Slag, manganese ore, magnetic susceptibility, magnetic separation

Acknowledgements

There are several people that I want to express my gratitude towards, for their help in the creation of this master's thesis.

Firstly, I would like to thank my supervisor Patrick Moldenhauer for his commitment and guidance throughout this work, without whom this project would not have been possible. I would also like to thank my examiner, Tobias Mattisson, who has been a valuable support in the completion of this thesis. Lastly, my gratitude also goes to Stefan Gustafsson and Duygu Yilmaz, for their help and tutorials in different analyzing techniques.

Frida Karlsson, Gothenburg, June 2019

Nomenclature

Acronyms

AR	Air reactor
CCS	Carbon capture and storage
CFB	Circulating fluidized bed
CLC	Chemical-looping combustion
FR	Fuel reactor
OC	Oxygen carrier
OCAC	Oxygen carrier aided combustion
SEM	Scanning electron microscopy
XRD	X-ray powder diffraction

Physical quantities

χ	Volume specific magnetic susceptibility	[-]
χ_{mass}	Mass specific magnetic susceptibility	$[\text{m}^3\text{kg}^{-1}]$
T_{N}	Néel temperature	[K] or [°C]

Contents

Chapter 1

Introduction

In the last hundreds of years, since the industrial revolution, our use of fossil fuels has continuously increased. The industrial revolution was a major turning point in our history: Suddenly we were able to travel faster and further than ever before, and production speeds soared. But in this new era, we became blind to the consequences our actions had; global warming and climate change. This has, however, begun to change. Sixty years ago, on the top of Mauna Loa in Hawaii, the CO_2 content of the atmosphere began to be measured. This record has shown that the current amount of CO_2 in the atmosphere, as well as the rate of increase, are greater than at any time in the past 800,000 years[1]. This accumulation of CO_2 has led to the increase of global temperatures; since the industrial revolution, the global temperature has increased by 0.8°C[2].

The change of Earth's climate results in melting of glaciers, rise of sea level, droughts and unstable weather. This will impact the lives of many people, particularly the poorer nations who do not bear the responsibility for the rise of global temperatures and who also have less capability to make a difference. Even in the best case scenario, i.e. if all greenhouse emissions were immediately stopped, the planet would increase to warm for a long time, due to the inertia of the climate system[1, 3]. In response to this, the Paris Agreement was adopted in 2015, with the intention to bring nations together in pursuit to limit the global temperature increase well below 2°C above pre-industrial levels. It was agreed upon that the global community should work towards limiting warming to 1.5°C [4].

Many countries have increased their use of wind and solar energy. But efforts are also being made to lower the CO_2 emission from the combustion of fossil fuels and enhancing its efficiency, as it is expected to remain a major energy source for a long time. This is mainly due to the abundance and that it is so well established. In order to reach the target of the Paris Agreement, active removal of CO_2 from the atmosphere is probably necessary[5]. This is possible with concepts like Carbon Capture and Storage (CCS), in which CO_2 is captured and transported to a location for storage. This concept can be divided into three categories; pre-combustion, oxy-fuel combustion and post-combustion.

Chemical-looping combustion (CLC) is a technology which falls into the oxy-fuel category and will be of consideration in this project. Here, oxygen instead of combustion air is supplied to the combustibles by a solid, so-called, oxygen carrier (OC). An oxygen carrier usually consists of metal-oxides that can exhibit magnetic properties. This will

be explored further in Section 2.2.1. CCS with fossil fuels could create a carbon neutral process, while CCS with biomass fuels could mean a reduction of CO_2 in the atmosphere, so-called negative emissions.

1.1 Scope

In this study, the magnetic properties of oxygen-carrying bed materials are studied with the aim to facilitate the determination of the magnetic fraction. This is important in order to increase recycling and reuse of these materials in combustion processes.

This work builds upon the resulting data in a Bachelor thesis from 2018, where magnetic fractions of three different oxygen carriers were recorded. In this work, correlations between their data and different material properties are explored in order to increase the understanding of the mechanism governing the magnetic behavior. And if possible, a model is to be established to predict the magnetic properties of oxygen carrying-materials based on, e.g., their elemental composition. Thus the aim of this project can be summarized as:

- Obtaining a better understanding of the mechanisms which govern the magnetic behaviour of oxygen carriers.
- If possible, construct a model with which the magnetic properties of oxygen-carrying materials can be predicted.

The scope of this study is limited to how the magnetic properties change over time for several well-known oxygen carriers, during usage in combustors utilizing these materials. The study will not go into detail of other imperative aspects of bed materials, such as their place in the redox cycle or economics. This project is also limited to the investigation of three types of bed material: ilmenite, LD Slag and Sibelco Calcined.

Chapter 2

Theory and Background

This chapter brings forth the underlying background and theory on which the project is based on. Firstly, the basics of combustion technology are given, followed by theory regarding magnetism. Lastly, the most relevant results of the proceeding Bachelor thesis, which this work builds upon, are described.

2.1 Circulating Fluidized Bed (CFB)

One possible design for a combustion power plant is the circulating fluidized bed (CFB) combustion unit, which is one of the branches of fluidized bed combustion (FBC). In FBC, the bed material (normally consisting of inert material like sand) and the fuel are brought into motion by inlets of combustion air situated at the bottom of the combustor (Figure 2.1). The bed material thus becomes fluidized. The distinctive aspect of a CFB process is that so much air is introduced through the nozzles so that the increased fluidization velocities enables the bed material to circulate throughout the whole combustor. A simplified schematic of this is shown in Figure 2.1, which also shows the cyclone that separates the bed material from the flue gasses before the bed material is reintroduced to the combustion chamber.[6]

In CFB combustion, the bed material increases the efficiency of the combustion by distributing heat across the combustor. It is also an advantage with respect to emissions of sulfur and nitrogen, which are normally low in such combustion systems.

Research has in recent years started looking at replacing the inert bed material with so-called active bed materials, i.e., bed materials with the capability to undergo oxidation and reduction at conditions present in the boiler. Such materials are usually called oxygen carriers (OCs). This has been shown to have several positive effects with respect to emissions and oxygen transfer in the bed[7, 8]. A technology that is based on CFB is chemical-looping combustion (CLC). This concept utilizes oxygen carriers to transfer oxygen between air and fuel, but here the oxidation and reduction are performed in different interconnected fluidized-bed reactors. The CLC concept will be explained further in Section 2.2.1.

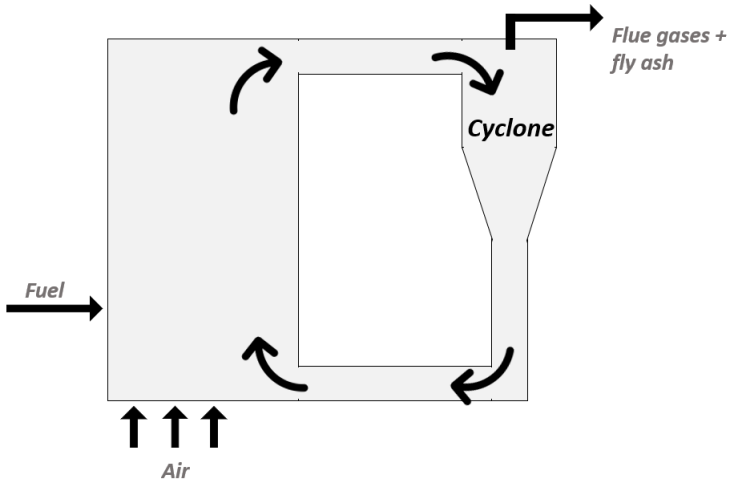

Figure 2.1: Simplified schematic of a CFB combustor, indicating how the bed material circulates in the combustion unit.

2.2 Oxygen Carriers

Ideally, oxygen carrying materials should fulfill a number of criteria; a high oxygen transfer capacity (i.e. a high maximum mass fraction of oxygen that can be transferred between the air and fuel reactors per cycle by the oxygen carrier[9]) and availability, to name a few. One of the reasons the oxygen carriers need to have a low cost is because they have a limited lifetime as the oxygen carriers undergo permanent stresses as a result of high temperatures with cyclic reduction and oxidation[9, 10]. This eventually leads to that the oxygen carriers needs to be replaced with new material. A continuous replacement of the bed material, a so-called make-up feed, is also required for commonly used bed materials, such as silica sand, that do not carry oxygen.

In the following sections chemical-looping combustion and oxygen carrier aided combustion – two combustion concepts that utilize oxygen carriers – will be described.

2.2.1 Chemical looping combustion (CLC)

A novel concept of combustion is chemical-looping combustion (CLC). This concept already started taking form in 1951 with Lewis and Gilliland's work on gasification of carbon by CO_2 in fluidized beds [11]. Still, most research has been performed in the last two decades.

In CLC units – unlike conventional combustion processes – the fuel is not oxidized by air but instead by oxygen bound to solids. These solids are called oxygen carriers and typically consist of metal oxides. The oxygen carrier is cycled through two interconnected fluidized bed reactors; the air reactor (AR) and the fuel reactor (FR), as seen in Figure 2.2. In the air reactor, the oxygen carriers are oxidized by air. The oxygen carriers are then separated from the air in a cyclone and transported to the fuel reactor (FR)

where combustion takes place. The reduced oxygen carriers subsequently return to the AR where the process starts over again. The advantage with this approach is that the combustion air and the fuel are never mixed, thus leading to that the CO_2 is obtained in a separate stream from N_2 (originating from the combustion air) and thus avoiding an expensive and energy-intensive gas separation. [12, 13]

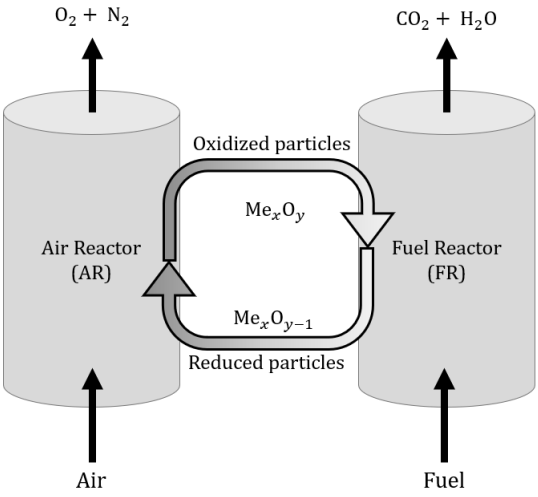

Figure 2.2: Schematic illustration of the CLC concept. Oxygen carriers are oxidized in the air reactor and transported to fuel reactor, where the fuel is oxidized. Reduced oxygen carriers then return to the air reactor, where they are oxidized again.

In Equation (2.1) below, the reduction and oxidation of metal oxides that occur in the two interconnected reactors are shown. Here $\mathrm{Me}_x\mathrm{O}_{y-1}$ is a reduced form and $\mathrm{Me}_x\mathrm{O}_y$ the fully oxidized oxygen carrier.

$$\begin{aligned}&\text{Reduction of oxygen carrier in FR:}\\ &\quad (2n+m)\mathrm{Me}_x\mathrm{O}_y + \mathrm{C}_n\mathrm{H}_{2m} \longrightarrow (2n+m)\mathrm{Me}_x\mathrm{O}_{y-1} + n\mathrm{CO}_2 + m\mathrm{H}_2\mathrm{O}\\ &\text{Oxidation of oxygen carrier in AR:}\\ &\quad \mathrm{O}_2 + 2\,\mathrm{Me}_x\mathrm{O}_{y-1} \longrightarrow 2\,\mathrm{Me}_x\mathrm{O}_y\end{aligned} \tag{2.1}$$

Since CO_2 in the CLC process is obtained as a separate stream, CLC is an excellent candidate for the carbon capture and storage (CCS) concept. The separation of CO_2, which can be expensive for other types of combustion processes, is avoided in CLC. With the use of fossil fuels, CLC in a CCS scheme would become carbon neutral and the use of biomass as fuel would lead to a reduction of atmospheric CO_2[5]. This is because biomass absorbs CO_2 during photosynthesis. With normal combustion, the CO_2 is returned to the atmosphere and from a system perspective would not contribute to any increase in the atmosphere. Still, if the CO_2 is stored, then a net-flow of CO_2 from the atmosphere would be achieved.

2.2.2 Oxygen Carrier Aided Combustion (OCAC)

Oxygen carrier aided combustion (OCAC) is an innovative concept with its foundation in CLC technology. OCAC is applied to the conventional fluidized bed combustor by replacing all or some of its bed material with oxygen carriers. An advantage with OCAC is thus that it is applicable to existing fluidized bed boilers without the need of any changes in the plant design[8]. With a bed material consisting of oxygen carriers in normal CFB combustion, not only is heat distributed across the combustor, but oxygen is also transported from oxygen-rich to oxygen-lean regions in the furnace, through continuous redox reactions[14]. In this way, an extra transport mechanism is introduced to the bed, which could compensate for inferior mixing in the bed. This further increases combustion efficiency and reduces the emissions as adequate mixing of fuel and oxygen during combustion is highly important [7, 15].

The application of this concept in a CFB was first performed at Chalmers in 2013 by Thunman et al. in a study in which they replaced 40 wt% of silica-sand bed material with ilmenite (an iron-titanium-based oxygen carrier). The study showed that ilmenite decreased CO concentration by 80% and NO concentration by 30% in comparison to operations with commonly used silica-sand[7].

As ilmenite, or any oxygen carrier, is more expensive than sand, it is important that the oxygen carrier can be reused or recycled. In any combustion process, such as OCAC or CLC, oxygen carrier will be lost through different mechanisms, for instance through elutriation and attrition. During the combustion process, the bed material also suffers contamination from fuel ash, which may change the efficiency of the oxygen carriers. This interaction with ash can also lead to agglomeration in which smaller particles clump together, creating larger particles. This may cause blockage of the air nozzles and/or passage ways[6], which heavily affects fluidization and/or circulation. It is thus important that the oxygen-carrying material can be separated from bed ash and other components and either returned directly or reused in granulation process, where new oxygen carriers can be made.

It has been shown that certain oxygen carriers are attracted by a magnet, and hence magnetic separation of particles, from ash, could be a way to increase efficiency and reuse of oxygen carriers.

2.3 Magnetism and Magnetic Susceptibility

Everything around us is magnetic. Though in some materials, like iron, this effect is more pronounced as the material can be seen rushing towards a magnet that is put next to it. Other materials like plastic do not seem to be magnetic at all, with no or small effects when in the presence of a magnet. The way in which substances react to the magnetic field of a magnet is measured as magnetic susceptibility. Magnetic susceptibility is a measure usually denoted with the Greek letter χ and is defined as the ratio between the magnetization M and the strength of the applied magnetic field H as stated

in Equation (2.2).

$$M = \chi H \tag{2.2}$$

The unit of magnetic susceptibility in Equation (2.2) is dimensionless and is more specifically called volume specific susceptibility. There are often times when it is more convenient to refer to mass specific susceptibility, χ_{mass}, in which the dimensionless quantity is divided by the material's bulk density. This is useful when comparing different measurements in which the density of the samples may vary. There are different categories a material can be placed in, depending on its magnetic susceptibility, such as ferromagnetic or diamagnetic. These will be explored in section 2.3.2.

2.3.1 The Source of Magnetism

Magnetism – and in extent magnetic susceptibility – of materials is an intricate phenomenon that is inseparable from quantum mechanics. Magnetic fields arise from the so-called magnetic moment, μ which is fully described in the realm of quantum mechanics. The source for the magnetic moment of an atom is threefold[16]:

(i) The spin of the electrons, S
(ii) The orbital angular momentum, L
(iii) The change in orbital momentum induced by applied magnetic field

The third source will be described in the next section in the discussion of diamagnetism. The first two are different kinds of electron motion and are visualized in Figure 2.3, each phenomena which has a magnetic moment associated with it. Source (ii) is easier to conceptualize of the two and is depicted in Figure 2.3 a), showing an electron rotating counterclockwise in a circular orbit around a nucleus. This can be seen as a circular electrical circuit which in turn creates a small magnetic field. The associated orbital magnetic moment, μ_{L}, can be seen as a vector quantity perpendicular to the plane of motion.

To conceptualize the electron spin, i.e. source (i), in a similar way is less intuitive since spin has no basis in classical physics. In Figure 2.3 b), an attempt to visualize the spin is shown. Here the electron's charge is distributed across a spherical surface where rotation of the charge would create tiny current loops, resulting in a magnetic moment, μ_{S}, along the rotation axis[17]. It is important to note, however, that this is merely an aid for visualization of spin: Electrons are not actual spheres, nor do they spin, i.e. rotate. The electron spin was, however, originally thought of as a rotation, and so the name "spin" remained. Intrigued readers are referred to literature, that address quantum physics, for further understanding (e.g. [17]).

All electrons in an atom have their own movement and vector quantity and contribute to the total magnetic moment of an atom. This can lead to either a cancellation of the total magnetic moment or a net magnetic moment[17]. By this, materials have a characteristic magnetic behaviour and may be placed in different categories, which will be explored in the following section.

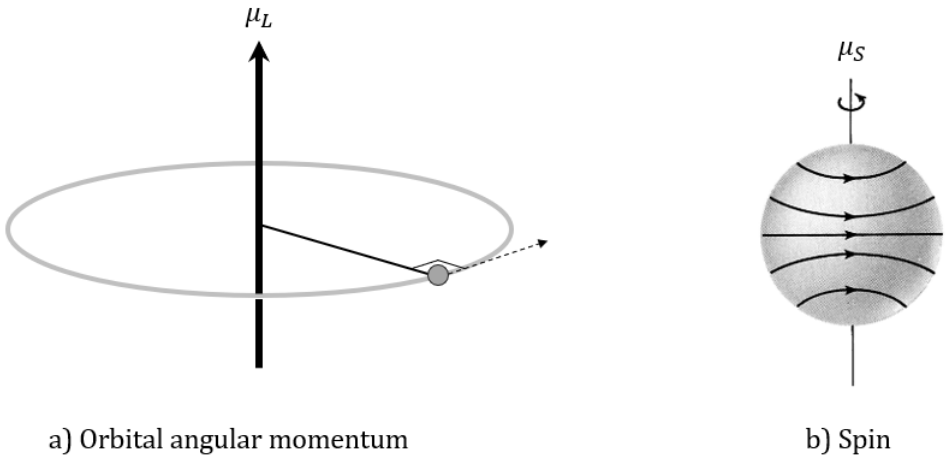

Figure 2.3: Visualization to the different motions of an electron. a) An orbiting electron around a nucleus resulting in an orbital angular momentum **L**. **b)** An aid to visualizing the spin of an electron. Note that the electron is rather a point and has no basis in classical physics. (Image b): Cullity and Graham[17])

2.3.2 Categorisation of Magnetic Behaviour

As an atom is made up of electrons, materials are in turn made up of many atoms with different numbers of electrons and therefore different magnetic behaviour, all contributing to the total magnetic behaviour. Materials can be placed in one of five different categories of magnetic behaviour; ranging from the most highly magnetic materials to those with, so to speak, negative magnetism. Below follows a discussion and explanation of the different forms of magnetism.

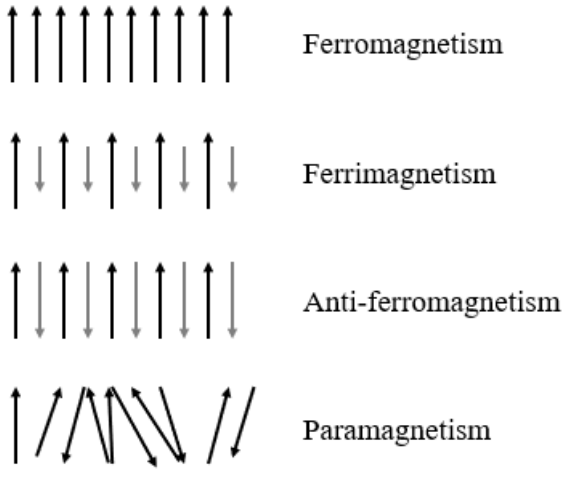

Figure 2.4: Schematic visualisation of the orientation of the magnetic moments in a applied magnetic field for the different categories of magnetic behaviour.

Ferromagnetism:
At one end of the magnetic spectrum, ferromagnetism is found. This category contains substances with very high magnetic susceptibility and that have a net magnetic moment

even when no field is applied. This suggests that all of the atomic magnetic moments have regular arrangements, see the schematic in Figure 2.4.[17] Some substances that fall into this category are pure iron, nickel and chromium[18]. A ferromagnetic material is not normally found in nature.

Ferrimagnetism:
Like ferromagnetic, ferrimagnetic substances' magnetic moments are strongly aligned but consists of two sets of forces that are opposing each other. These forces are unequal, however, and result in a net magnetic moment, see Figure 2.4. Like ferromagnetic materials, ferrimagnetic substances exhibit a spontaneous magnetization at room temperature. In this category magnetite (Fe_3O_4) is found, which is a common mineral found in all igneous rocks and will be returned to several times in this report.

Antiferromagnetism:
Lower magnetic susceptibility than that of ferromagnetic is found for antiferromagnetic substances. These exhibit a small positive susceptibility at all temperatures. The magnetic moments are aligned in a similar fashion as ferrimagnetic substances but have the properties that these opposing forces virtually cancel each other out[18], see Figure 2.4.

The magnetic susceptibility of antiferromagnetic materials depends on the temperature in a way so that the substances behaves as a paramagnetic material (less magnetic materials which will be explained shortly) above a critical temperature called the Néel temperature, T_{N}, and antiferromagnetic below T_{N}[17]. Manganese oxide (MnO), for example, is an antiferromagnetic material with $T_{\mathrm{N}} = -151^{\circ}\mathrm{C}$, and will therefore appear as a paramagnetic substance at room temperature. Another antiferromagnetic material that will be considered in this report is hematite (Fe_2O_3).

Paramagnetism:
Magnetically weaker (or similar) than antiferromagnetic substances are paramagnetic substances. With no applied magnetic field, the atomic magnetic moments point at random and cancel each other out, so that there is no net magnetic moment (i.e. the magnetization of the specimen is zero). When an external field is applied, however, there is a tendency for the atomic moment to turn towards the direction of the field. But the thermal agitation of the atoms opposes this tendency and tends to keep the atomic moments pointed in random directions. Thus the result is only a partial alignment in the field direction and therefore a small positive susceptibility is obtained, see Figure 2.4. [17]

Diamagnetism:
Diamagnetism is a universal property originating from Source (iii) mentioned above. This arises in the presence of a changing magnetic field and contributes to negative magnetic susceptibility: Orbiting electrons are electrical circuits and when a magnetic field is applied it follows from Lenz's law that the electrons will induce their own magnetic field as to oppose the flux change leading to a negative magnetic moment.

Any paramagnetic or ferromagnetic behaviour in an atom would always dominate, so the purely diamagnetic substances are those, such as monoatomic closed-shelled gases, which exhibit no net magnetic moment in the absence of a magnetic field. [17]

2.3.3 Magnetic Susceptibility in Mixtures of Minerals

In theory, it is possible to predict the magnetic susceptibility of a substance by adding the susceptibility of every component in that substance. This is often not a feasible approach, but as John Dearing explains in *Environmental Magnetic Susceptibility*[18], simplifications can be made by determining the components which are more significant in the material.

Ferrimagnetic substances like magnetite can be about 1000 times more magnetic than antiferromagnetic substances. Even in very small amounts, a ferrimagnetic component would dominate the total magnetic susceptibility of a sample of mixed materials (unless the sample is contaminated by ferromagnetic materials, which is rarely the case in nature). In his book, Dearing describes a hypothetical substance that contains 0.1% magnetite and 90% paramagnetic minerals. The small amount of magnetite would provide about 84% of the total susceptibility while the paramagnetic minerals only provide about 6%.[18]

By this reckoning, it is possible to estimate the concentration of the most significant component in a mixed substance by dividing the sample's total susceptibility by the individual substance included in the sample. In Equation (2.3) this is given for magnetite included in a mixture.

$$\text{Estimated concentration of magnetite} = \frac{\text{Sample's bulk susceptibility}}{\text{Magnetite's susceptibility}} \tag{2.3}$$

In Table A.1 in the Appendix the reader can find Dearing's table of magnetic susceptbility of a range of different materials.

2.4 The Preceding Study

As mentioned above, this work relies on a bachelor's thesis conducted in 2018. In that project, the possibility to recycle oxygen carriers by separating the magnetic – from non-magnetic – fraction of different bed materials obtained from different combustion processes using a magnetic separator was investigated. Several different samples were investigated, retrieved both from CLC and OCAC operations. That project also aimed to construct a model by which the magnetic fraction of other oxygen carriers could be predicted.

The materials retrieved from different units were iron- and manganese-based materials, which had been exposed to different types of fuels. Thus they could, in some cases, contain ash fractions. The main method used to separate the magnetic fraction from the non-magnetic fraction was to let the bed material travel along a band feeder equipped with a magnetic roll. The schematic in Figure 2.5 shows how the magnetic particles (in black) travel along a different path than the non-magnetic particles. Both types of particles are collected in containers separated by a splitter.

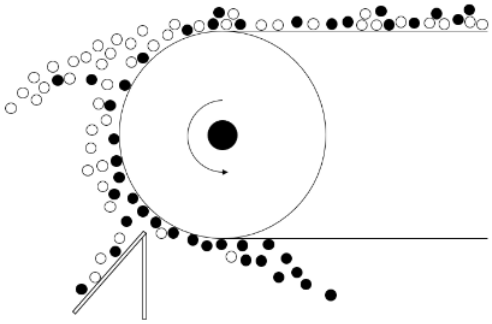

Figure 2.5: Schematics over a band feeder. The band goes over a magnetic roll which the magnetic particles (black) becomes attracted to. The non-magnetic particles are shown in white. (Image: Andersson et al.[19])

Three different materials were investigated; LD Slag, ilmenite and Sibelco Calcined, each with several different samples taken from different combustion units and usage times. LD Slag and ilmenite are materials with considerable content of iron (e.g., ilmenite contains around 37 mass% iron), while Sibelco Calcined is a manganese ore, which contains much less iron, i.e. around 6 mass%.

Their measurements of the magnetic fraction showed that LD Slag, after use, could be separated up to 95% on a mass-basis, ilmenite 70-90% and Sibelco Calcined 5-7%. A bar diagram of their results are also shown in Figure 2.6 and will be referred to later in this work. One conclusion was that Sibelco Calcined was not suitable for magnetic separation due to its low magnetic fraction. But several of the results were difficult to explain and the underlying reason for the differences was not determined. Neither could a model for the prediction of magnetic fraction be established.

It is therefore the ambition of this master's thesis to further investigate these oxygen carrier materials to obtain a better understanding of the mechanisms and parameters that govern magnetic separation, and, if possible, create a model.

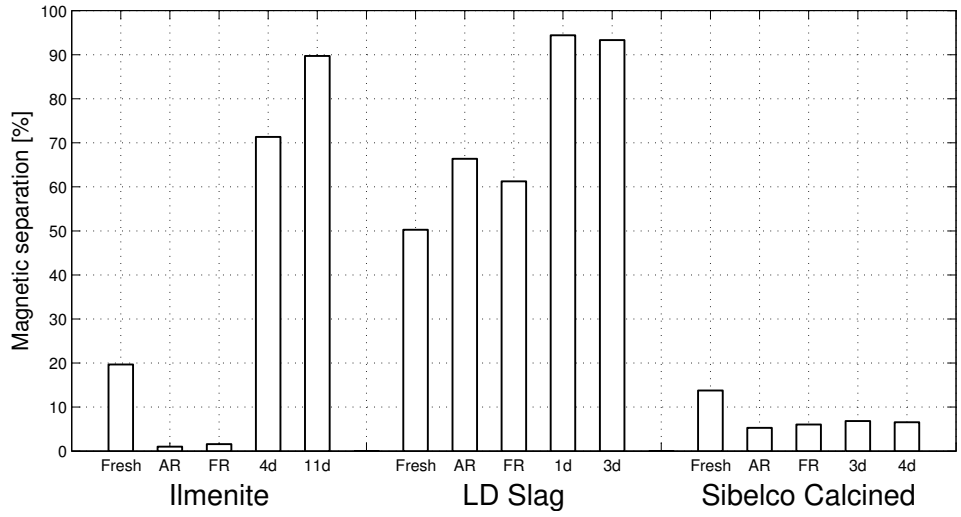

Figure 2.6: Magnetic separation degree bar diagram of data obtained in 2018, showing the magnetic fraction for all different samples of oxygen carriers studied in this work. (Raw data from Andersson et al.[19])

Chapter 3

Investigated Oxygen Carriers

The aim of this work is to increase the understanding of the mechanisms and parameters which govern magnetic separation, more specifically around common iron- and manganese-based materials. This will be done by utilizing a number of experimental methods, including SEM and elemental mapping with EDX, in addition to measurements of magnetic susceptibility.

While oxygen carriers are the main focus in this work, the magnetic properties of their active components will also be studied. Thus, the substances that will be investigated in this work are:

- ➔ **Oxygen carriers:** The same iron- and manganese-based oxygen carriers that were investigated in the bachelor's thesis: Ilmenite, LD Slag and Sibelco Calcined.
- ➔ **Pure metal-oxides:** Different iron- and manganese-oxides that may occur in the investigated oxygen carriers – either in "fresh" or "used" state.

The three types of oxygen carriers that are analyzed in this work are ilmenite, LD Slag and Sibelco Calcined. These are all in powdered form with particle size in the range $100 - 400\,\mu\mathrm{m}$. For each type of oxygen carrier there are five samples (see Table 3.1) that are measured throughout this work:

- One fresh, unused sample that is used as a reference.
- Two samples that have been used in a 12 MW CFB combustor for OCAC operation, where samples have been extracted from the bottom of the combustor after different duration at temperatures around 800-850°C.
- Two samples that have been used in CLC operation, from either a 10 kW or a 100 kW unit, at around 900-950°C in an oxidized state. One of these two samples is taken from the air reactor and the other from the fuel reactor.

In the following sections, each of these bed materials is described, starting with the two iron-based oxygen carriers followed by the manganese-based oxygen carrier. A summary of the elemental composition of the three oxygen carrier materials is given in Table 3.3.

The pure metal-oxides investigated in this work are shown in Table 3.2 and have a purity

Table 3.1: Sample specification of the analysed oxygen carriers.

	Signature	Power (Facility)	Fuel	Duration
Ilmenite	il-OCAC/4d	12 MW (OCAC)	Wood chip/pellets	4 days
	il-OCAC/11d	12 MW (OCAC)	Wood chips/pellets	11 days
	il-CLC/FR	10 kW (CLC FR)	Diesel, vacuum residue	76 hours
	il-CLC/AR	10 kW (CLC AR)	Diesel, vacuum residue	76 hours
	il-Fresh	–	–	–
LD Slag	LD-OCAC/1d	12 MW (OCAC)	Wood chips/pellets	1 day
	LD-OCAC/2d	12 MW (OCAC)	Wood chips/pellets	2 days
	LD–CLC/FR	10 kW (CLC FR)	Wood pellets	28 hours
	LD-CLC/AR	10 kW (CLC AR)	Wood pellets	28 hours
	LD-Fresh	–	–	–
Sibelco Calcined	SIB-OCAC/3d	12 MW (OCAC)	Wood chips/pellets	3 days
	SIB-OCAC/4d	12 MW (OCAC)	Wood chips/pellets	4 days
	SIB-CLC/FR	100 kW (CLC FR)	Coal, wood coal/pellets	34 hours
	SIB-CLC/AR	100 kW (CLC AR)	Coal, wood coal/pellets	34 hours
	SIB-Fresh	–	–	–

of about $97-99\%$. These samples were also much finer (ca $50\,\mu m$) than the particle size of the bed material (ca $100-400\,\mu m$). Not all phases detected in the oxygen carrier samples were measured. Wüstite (FeO) would only be formed in highly reducing conditions and is therefore believed to be of little significance.

Table 3.2: Pure metal-oxides that are measured. Some of the different oxidation phases of the oxygen carriers.

Iron oxides	Manganese oxides
Fe_2O_3 (hematite)	MnO_2
Fe_3O_4 (magnetite)	Mn_2O_3
	Mn_3O_4
	MnO

3.1 Fe-based Oxygen Carriers

Of the three oxygen carrier materials investigated, two of them have high concentrations of iron. As can be seen in Table 3.3 these are ilmenite and LD Slag. As described, under combustion processes iron would undergo oxidation and reduction. The possible oxidation states of iron are seen in Equation (3.1), going from most reduced to fully

Table 3.3: Elemental composition in decreasing abundance of the three types of oxygen carriers investigated (without oxygen). Elements with mass- or atomic percentages under 1 are omitted.

Ilmenite			**LD-slag**			**Sibelco Calcined**		
	(mass %)	(atom %)		(mass %)	(atom %)		(mass %)	(atom %)
Fe	**37**	**48**	Ca	27	47	**Mn**	**46**	**63**
Ti	27	41	**Fe**	**14**	**17**	**Fe**	**6**	**8**
Mg	2	7	Mg	6	17	Al	4	12
			Si	5	12	Si	3	9
			Mn	2	3	Ca	2	4

oxidized.

$$\underset{\text{Iron}}{\text{Fe}} \longrightarrow \underset{\text{Wüstite}}{\text{FeO}} \longrightarrow \underset{\text{Magnetite}}{\text{Fe}_3\text{O}_4} \longrightarrow \underset{\text{Hematite}}{\text{Fe}_2\text{O}_3} \tag{3.1}$$

As mentioned above, the two most oxidized phases of iron are antiferromagnetic and ferrimagnetic and would therefore dominate the overall magnetic behaviour of a sample if they are present. Wüstite (FeO) is also antiferromagnetic but has a Néel temperature around $T_\text{N} \approx -70°\text{C}$ and behaves therefore de facto as a paramagnetic substance[20]. The antiferromagnetic hematite, on the other hand, has a Néel temperature of around $T_\text{N} \approx 675°\text{C}$ and will thus retain it's antiferromagnetic behaviour at room temperature.

Hematite and magnetite are also the forms which are expected to be dominant in a combustion process, although lower oxidized forms could be formed locally in the combustor. Therefore iron will be a very important element in the study of these oxygen carriers.

3.1.1 Ilmenite

Ilmenite is a naturally occurring ore found in metamorphic and igneous rocks (i.e. solidified molten rock material[21]) with the chemical formula FeTiO_3. Ilmenite is also the name of one of the three oxygen carriers studied in this work and contains large amounts of this mineral.

The reduced form of ilmenite is FeTiO_3 ($\text{FeO}\cdot\text{TiO}_2$), where the iron oxide is the active component of the mineral with the primary oxygen carrying capacity. The oxidized form is Fe_2TiO_5 ($\text{Fe}_2\text{O}_3 \cdot \text{TiO}_2$). The metal ions alternate between layers of Ti^{4+} and Fe^{2+} ions where the iron layers are antiferromagnetic while the titanium layers do not contribute to the magnetic moment [22].

Ilmenite's role as an oxygen carrier has been explored on numerous occasions before, which has shown that it's reactivity increases with increasing redox cycles until it reaches a maximum reaction rate[23]. The ilmenite particles also become more porous after a number of redox cycles, and it has been suggested that this increase of reaction surfaces is the cause for higher reactivity.[24] It has also been also that a migration of iron

and titanium occurs, leading to the formation of an iron-rich shell and a titanium-rich core[25].

3.1.2 LD Slag

For every tonne steel produced, 2 to 4 tonnes of waste are generated. Among the waste, LD Slag emerges. The name comes from the Linz-Donawitz (LD) process, in which scrap- and pig iron is processed into steel. The composition of these slags varies greatly depending on where they are generated, but common components are calcium and iron, as well as manganese to some extent[26]. The active components of LD Slag, governing its oxidation capacity, are iron oxides and manganese oxides, though iron is usually the more abundant material in LD Slag[8].

3.2 Mn-based oxygen carrier: Sibelco Calcined

Sibelco Calcined is a material made from manganese ore and is produced by the company Sibelco. Calcined referrers to the process in which solid materials are heated to high temperatures (without melting).

Manganese-based materials are of interest as they are cheap, non-toxic and have a high oxygen transfer capacity, and are thus highly suitable for use in CLC and OCAC. The material has been identified as a promising oxygen carrier material due to its high oxygen transfer capacity compared to iron-based oxides, i.e. 7-10 wt% compared to 3.3 wt% for iron oxide[27–29]. The high oxygen transfer capacity of manganese-based materials is due to the possibility of full conversion of fuel for both the reduction of Mn_2O_3 to Mn_3O_4 as well as Mn_3O_4 to MnO. Iron-based oxygen carriers on the other hand are limited to the reduction of hematite to magnetite if you want to achieve full conversion of the fuel.[8] In Equation (3.2) the different oxidation states of manganese are shown.

$$\mathrm{MnO} \longrightarrow \mathrm{Mn_3O_4} \longrightarrow \mathrm{Mn_2O_3} \longrightarrow \mathrm{MnO_2}\,, \tag{3.2}$$

It is highlighted that manganese ores, like many other ores, are far from pure, and that the manganese species can form other mixed oxide phases, for instance Mn-Fe- or Mn-Ca-based oxides.

Chapter 4

Methodology

The methodology of this work was split into three paths, each analyzing certain properties of the oxygen carriers. The first method is the quantification of magnetic susceptibility. After this, analyses based on SEM and XRD are described.

For each of these analyzing methods, a brief introduction to the instrument used is given, followed by how the measuring method was developed along with tests that were made. Lastly, the final method procedure is described.

4.1 Magnetic Susceptibility

To measure magnetic susceptibility, Bartington MS2 Susceptibility System was used with a MS2B Dual Frequency Sensor. The sensor accepts a sample volume of about 10 ml where measurements can be made in magnetic fields generated at either 0.46 kHz or 4.6 kHz. This sensor has therefore the ability to measure whether the susceptibility at these frequencies differs, in which case there is an indication of ultrafine ferrimagnetic particles ($< 0.03\,\mu\mathrm{m}$). This is however not of interest for this work. The equipment is controlled through the software Bartsoft.

During a measurement, a magnetic field is created at the selected frequency and the magnetization of the sample is recorded at room temperature. The ratio between the magnetization and the strenght of the applied field is calculated in accordance with Equation (2.2). The obtained value is volume specific magnetic susceptibility which later can be converted to mass specific magnetic susceptibility.

4.1.1 Method Development

As the sample volume is used in the conversion to mass specific susceptibility, an error that could occur is that the sample pot is not properly filled. The severity of a deviation from exactly filled pots was tested by conducting five measurements on the same substance, filled to varying degrees (but all close to filled or pressed down). The resulting volume specific susceptibility was divided by the density (where the same volume had been used regardless of actual volume). This resulted in rather similar values, i.e., the

standard deviation was less than 5% of the mean, which indicated that non-perfect filled pots are not detrimental to the measurements. Despite this, the pots were still filled carefully during the measurement procedure.

4.1.2 Measurement Procedure

For a measurement of magnetic susceptibility using a MS2B sensor, a 10 ml plastic pot was filled to the brim with a powder sample and excess material was scraped off. The net mass was recorded (i.e. without the mass of the plastic pot) for the later conversion to mass specific susceptibility. The filled pot was placed in the sensor and measured during 10 seconds at low frequency and the volume specific susceptibility was obtained. This value was then divided by the calculated density as to obtain mass specific susceptibility as in Equation (4.1). The same procedure was performed three times for each sample (with the pot filled anew) and an average was obtained. The standard deviation between the three measurements was usually below 1% of the mean, which made repetitions largely unnecessary.

$$\chi_{\text{mass}} = \frac{\chi}{\rho} \tag{4.1}$$

Measurements were also made on the pure metal oxides which can occur in the bed samples (see Chapter 3). These are expected to give a good basis for comparison with the oxygen carriers. These phases were given in Table 3.2.

4.2 Analysis of Phase Composition Using XRD

In this project, X-ray powder diffraction (XRD) was used to determine what changes in composition occur in the oxygen carriers as they are exposed to redox reactions in the combustor. This was done in order to see whether a correlation between phase and magnetic properties exists. Note that with the equipment used here only information on which phases are present could be obtained, not in what quantity. Further, only crystal phases can be identified, and any amorphous or glassy phases cannot be determined with this XRD analysis.

This technique makes use of the interaction between applied monochromatic light (photons) and electrons in the material. This interaction can be elastic, in which incident photons do not lose energy or inelastic in which they do lose energy. In a lattice, this results in constructive or destructive interference, depending on whether the scattered waves are in- or out of phase [30]. Constructive interference occurs for angles θ for which Bragg's law is fulfilled:

$$n\lambda = 2d\sin\theta\,,$$

where n is the order of reflection, λ the wavelength of the incident X-ray, d the crystal lattice planar distance and θ is the scattering angle. See also Figure 4.1. The diffracted X-

rays are detected and counted, and a spectrum over a range of 2θ-angles is created [31]. The produced diffraction pattern will contain a series of peaks that are characteristic for a certain phase/material. By comparing an obtained diffraction pattern to the pattern of known samples, identification of the phase can be made by comparison to reference materials in a database.

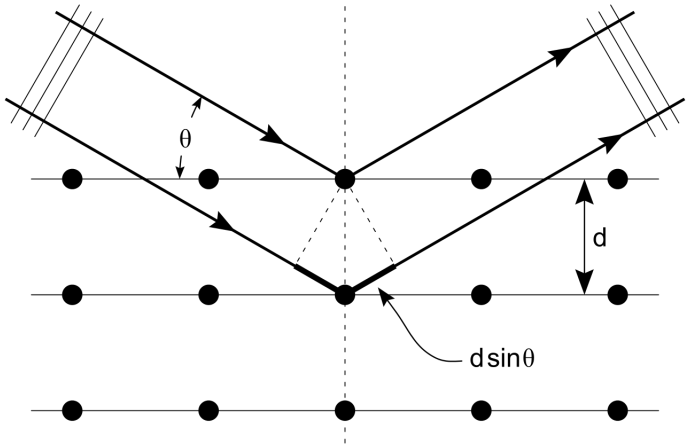

Figure 4.1: Diffraction of incoming parallel X-rays.(Image: Hydrargyrum)

The analysis was made with a D8 ADVANCE diffractometer and a LYNXEYE detector, that collects data at a range of angles pre-determined in the corresponding software. The obtained data is analyzed with the software EVA (short for evaluation) where the obtained diffraction spectra are compared to diffraction patterns of known compounds from a database.

4.2.1 Method Development

The two factors that affect the quality of an XRD measurement the most are the preparation of the sample and the measurement parameters appointed in the software. Ideally, this yield a diffractogram with a high signal-to-noise ratio and a clear baseline, provided that the phases are crystalline. This is then followed by the interpretation of the peaks, which can be challenging, for heterogeneous materials, and which will be revisited in Section 4.2.2.

4.2.1.1 Sample Preparation

Only a small amount of a few millilitres is needed for a XRD measurement. The way that the powdered sample is prepared in the sample holder is important as it is vital that the surface of the sample is as flat as possible. This is because the XRD approximates the sample with an infinite lattice, not a collection of small particles. For this reason, it is also recommended that the particle size is small (less than around $50\,\mu\mathrm{m}$) as this creates more particles with the expected orientation and the characteristic peaks are increased in intensity and decreased in width.

Since the particle size of the samples analyzed in this work ranges between around 100 and $400\,\mu\mathrm{m}$, a sample was crushed and resulting spectra compared with a non-crushed sample of the same kind. The improvement of the spectra were rather small, and it was deemed that the non-crushed samples was adequate for this analysis, as this would also save time.

Normally a glass plate is used to press down the sample to ensure a flat surface, for these measurements, however, it was found that the sample had a tendency to stick to the glass by static electricity. Therefore a metal spatula was used instead.

4.2.1.2 System Parameters

The other factor that directly affects the quality of a measurement, is the system parameters that are given to the diffractometer. This is done in the software XRD-Wizard where a number of conditions can be assigned. Here, a voltage of 40 kV and a current of 40 mA were also assigned for the X-ray source. The parameters that were mostly considered were Step Size and Time/Step. The step size is the interval of 2θ at which the data is acquired, where a smaller step size is more accurate but also results in more noise in the data (at a small scale). The time per step is the scanning speed, i.e. the time data is collected at each angle, where longer time per step leads to higher counts and more accurate data, i.e., a higher signal-to-noise ratio. High quality is paid in time, as measurements easily can take up to an hour. When a multitude of samples is to be analyzed, compromises must be made.

While holding the time/step fixed, the step size was put to 0.1, 0.05 and 0.013° and the acquired diffraction patterns were observed which lead to the decision that a step size of 0.05° was found adequate. One and two seconds was tested with the selected step size (where the latter is rather high in this regard). Here two seconds were selected.

4.2.2 Measurement Procedure

Each sample was carefully prepared in a sample holder as described in Section 4.2.1.1 and placed into the instrument with the following system parameters:

Step size: 0.05°
Time/step: 2 seconds
Voltage: 40 kV
Current: 40 mA

When analysing the first of the five samples of either ilmenite, LD Slag or Sibelco Calcined, the analysis was made over a wide range of 10-90°. If the characteristic peaks of important phases were then found in a more narrow range, the following measurements on that oxygen carrier would be made in this smaller range. This is because all samples of the same oxygen carrier are expected to have characteristic peaks in similar places as they have similar compositions. This would also save time.

As mentioned before, the evaluation of the data can be quite tedious. The obtained diffractogram is automatically analysed and compared to a multitude of diffractograms of known samples. It is then up to the user to narrow it down and determine which phases are more probable for the analysed sample. This can be difficult at times, especially when the substance contains many elements and/or has amorphous regions. As an example, the diffraction patterns of ilmenite and LD Slag are shown in Figure 4.2. This may give the reader an impression of the varying difficulty one could have when analyzing a diffraction pattern. In this figure, ilmenite has clear characteristic peaks, while those of LD Slag are more difficult to identify.

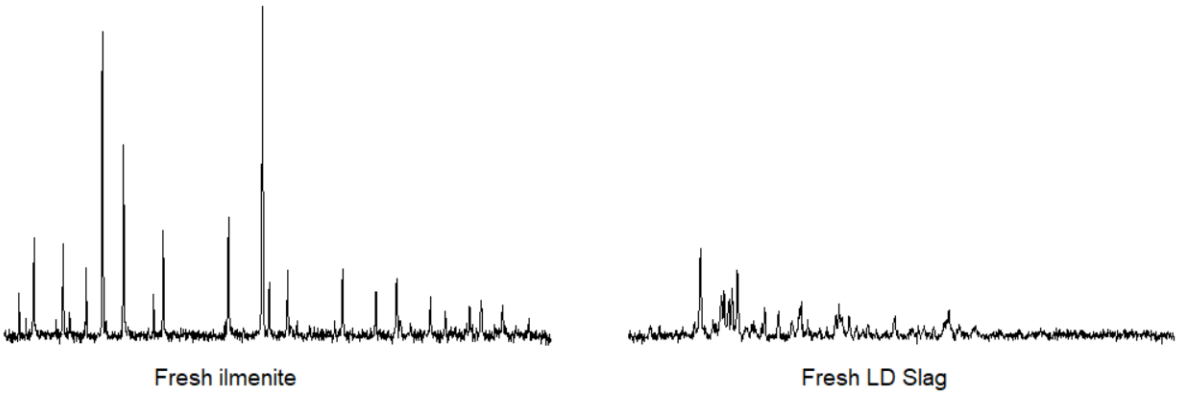

Figure 4.2: Examples of different diffraction patterns. Here fresh ilmenite has clear defined characteristic peaks, while the characteristic peaks of fresh LD Slag are less clear. Both diffractograms have the same intensity range on the vertical axis.

4.3 Elemental Analysis Using SEM–EDX

In this work, scanning electron microscopy (SEM) has been used to acquire images of particles and energy dispersive X-ray spectroscopy (EDX or EDS) has been used to determine which elements are present in the material and how the elements are distributed across the surface of the particles. The results are used as a complement to the XRD analyses.

In SEM, the sample is placed in a vacuum where a focused beam of electrons scans across the surface. The interaction between the electrons and the substance's atoms at various depth give rise to different types of signals. Among the different types of signals are backscattered electrons (BSE) and secondary electrons (SE). The former originates from the primary electrons from the incident beam that is, as the name suggests, scattered back. The latter, SE, are the samples own valence electrons that are energized by the electron beam to a point where they leave the atom. Both BSE and SE gives information about the surface topography.

Apart from BSE and SE, the analyzed substance will also give rise to X-rays. These arise as a result of the process in which core electrons are knocked out by the electron beam and subsequently replaced by electrons originating from outer shells. When these

electrons move to lower energy levels, energy is emitted in the form of characteristic X-rays. An important difference between XRD and EDX is that the former can give information regarding the actual crystalline phase, while the latter is used to identify the elements present, independent of form.

For this work, SEM (FEI Quanta 200 field emission gun ESEM) was used together with INCA EDX system for elemental analysis.

4.3.1 Method Development

The analyzed particles are relatively big (for this kind of analysis) a particle that had a flat facet towards the beam was sought. In this way, more of the particle could be in focus at the same time and a better EDX analysis could be made. When a suitable particle was found and brought to the EDX system, an analysis could be made over the entire particle, a so-called map-analysis. In this way a number of different images were created that showed different elements and their location on the surface of the particle.

In the software, the acquisition time of the data is chosen. Long acquisition time increase the energy resolution, but too long X-ray acquisition time may damage the sample and may also lead to degraded spatial resolution due to drift and contamination.[32, 33] During the acquisition of data, a live image of the energy spectrum is shown. This EDX spectrum is initially very unstable, but stabilizes as more data is acquired. Some sources claim that "enough" data has been acquired when spectrum is steady, as a rule of thumb[33]. This also depends on what accuracy is desired.

In order to test how long the total acquisition time should be, a site was selected on an LD Slag particle (LD-OCAC/1d) and two measurements were performed with a total acquisition time of 10 respective 90 minutes. The obtained spectra for these measurements were then plotted and superimposed (after normalisation) so that any difference would be clear. The result of this is seen in Figure A.1 in Appendix, where it is clear that the difference between these different acquisition times is negligible. Here, it was assessed that an acquisition time of 10 minutes would be enough for this sample.

There is however another property of a longer acquisition time that is of interest. That is the visual aspect of a map analysis. The purpose of creating maps of the present elements is mostly for the visual representation of the distribution and an overly resolved image does not give much advantage over a lesser resolved one. Even though adequate data was obtained after 10 minutes, the final acquisition time of 15 minutes was deemed suitable.

4.3.2 Measurement Procedure

The powdered sample is attached to a mount with carbon adhesive tape and placed into the instrument. A connected computer is used to focus the electron beam on the sample, with a voltage of 20 kV. When a satisfactory site had been found, an EDX computer is used to import this image and the analysis is made with an acquisition time of about 15

minutes.

Cross-sections of two samples of LD Slag[1] were also analyzed. These samples had been mounted in epoxy resin, ground and polished to expose the cross-section of the particles. Of the two samples analyzed one was unused LD slag and the other one particles from a batch taken after 65 hours in OCAC operation. These samples were also covered with a thin layer of gold that had been sputtered on to ensure that the particles did not become overcharged as the surrounding epoxy is not electrically conducting.

[1]Provided by Fredrik Hildor

Chapter 5

Results

In this chapter, different results obtained by the different analyzing techniques are presented. This chapter will also include some interpretations of the results and how they are connected. At the end of each section, an intermediate summary will be given where the major conclusions are stated as well as questions that have arisen. The questions will be answered by the result of other analyzing techniques and/or will be discussed in Chapter 6. For more extensive discussion and clarifications, the reader is referred to Chapter 6 where further connections will be made with other studies.

Firstly, the outcomes of the measurements of magnetic susceptibility and the different results related to this will be presented. Thereafter the results obtained from the XRD- and SEM–EDX-analyses will be shown.

5.1 Magnetic Susceptibility

In this section different results related to magnetic susceptibility are presented. First the magnetic behaviour of reference material – pure iron- and manganese-oxides, common in the studied oxygen carriers – are presented. Thereafter the magnetic behaviours of the oxygen carriers are presented.

5.1.1 Magnetic Behaviour of Pure Fe- and Mn-oxides (reference materials)

As discussed in Chapter 3, the magnetic properties of the oxygen carrier materials are, to a large extent, governed by the common transition metal oxides. The results of the mass specific susceptibility of these are presented in Table 5.1.

Of the different phases analyzed, magnetite (Fe_3O_4) stands out with its high magnetic susceptibility; 75 times greater than the runner-up, hematite (Fe_2O_3). This was an expected result as magnetite is known for its magnetic properties. The recorded susceptibility value for magnetite is comparable to that presented in Dearing's handbook which is stated in Table 5.1.

Table 5.1: Mass specific magnetic susceptibility of pure oxide phases. Values of magnetic susceptibility measured for different pure iron- and manganese oxides, common in the studied oxygen carriers.

Phase	χ_{mass} $(10^{-6}\ \text{m}^3\text{kg}^{-1})$
Fe_2O_3 (hematite)	8.96 †
Fe_3O_4 (magnetite)	657.51 ‡
MnO_2	0.25
Mn_2O_3	0.75
Mn_3O_4	0.54
MnO	0.61

†...Dearing: $(0.3 - 1.7) \times 10^{-6}\ \text{m}^3\text{kg}^{-1}$
‡...Dearing: $(390 - 1000) \times 10^{-6}\ \text{m}^3\text{kg}^{-1}$

The magnetic susceptibility of wüstite (FeO) was not measured. No mass specific susceptibility has been found in literature. But as described in Section 3.1, wüstite behaves as a paramagnetic substance at room temperature and is therefore expected to be less magnetic than hematite and magnetite.

Magnetite was referred to in Section 2.3.3 as being able to completely dominate the total susceptibility reading of a sample, even if only present in small amounts. The same can be suggested to happen to the oxygen carriers studied in this work, for which susceptibility will be presented in the following section. And from this, it can be suggested that an ideal iron-based oxygen carrier – in the context of magnetic separation – should contain some quantity (the more the better) of magnetite at the point of extraction from the combustor.

Since magnetic susceptibility is an additive quantity, it can also be suggested from these results that a mixed material measuring higher than about $9 \times 10^{-6}\ \text{m}^3\text{kg}^{-1}$, should contain some quantity of magnetite. This is because no amount of hematite (the second most magnetic phase here) can exhibit a higher value than this.

From Table 3.2 we also see that the various manganese-oxides have relatively low susceptibilities and would by this reckoning not be suitable for magnetic separation. It should be mentioned, however, that most manganese ores do contain relatively high fractions of other metals, especially iron. This means that the overall magnetic susceptibility of materials made from manganese ores can be higher than that of the different manganese oxides.

5.1.2 Magnetic Behaviour of Oxygen Carriers

In Table 5.2, the mass specific magnetic susceptibility of the different oxygen carriers is presented. A bar diagram of this is also shown in Figure 5.1. From this we can see

Table 5.2: Mass specific magnetic susceptibility of OC.

Sample		χ_{mass} $(10^{-6}\ m^3kg^{-1})$
Ilmenite	Fresh	3.55
	CLC/AR	0.77
	CLC/FR	0.75
	OCAC/4d	29.33
	OCAC/11d	47.41
LD Slag	Fresh	17.37
	CLC/AR	43.31
	CLC/FR	41.51
	OCAC/1d	88.29
	OCAC/2d	77.63
Sibelco Calcined	Fresh	15.62
	CLC/AR	11.52
	CLC/FR	11.38
	OCAC/3d	12.88
	OCAC/4d	11.86

that of the three oxygen carriers, Sibelco Calcined is the most stable material, and has relatively similar magnetic susceptibility for all of sample. In contrast, ilmenite shows a clear increase in susceptibility after use in the OCAC process, but a decrease with respect to the samples from CLC. The fact that Sibelco Calcined is unable to achieve the high values seen with some ilmenite samples is in alignment with the conclusion drawn in the previous section, which suggests that this manganese-based oxygen carrier would measure lower in magnetic susceptibility since it does not contain any large amounts of iron. In Table 5.2 we also see, however, that the magnetic susceptibility of ilmenite samples decreases after use in the CLC facility which will need to be explained later.

From the findings in the previous section, it could be suggested that all samples in Table 5.2 with a mass specific susceptibility higher than $9 \times 10^{-6}\ m^3kg^{-1}$ contain at least some quantity of magnetite. The different Sibelco Calcined samples would in this reckoning only contain a very small amount of magnetite, while some of ilmenite and LD Slag samples should contain a rather large amount. The susceptibility of hematite and magnetite are shown with horizontal lines in Figure 5.1.

It should be mentioned that these conclusions are made with the basis of the different iron- and manganese-oxides measured. The oxygen carriers contain many other compounds, for which magnetic susceptibility has not been measured.

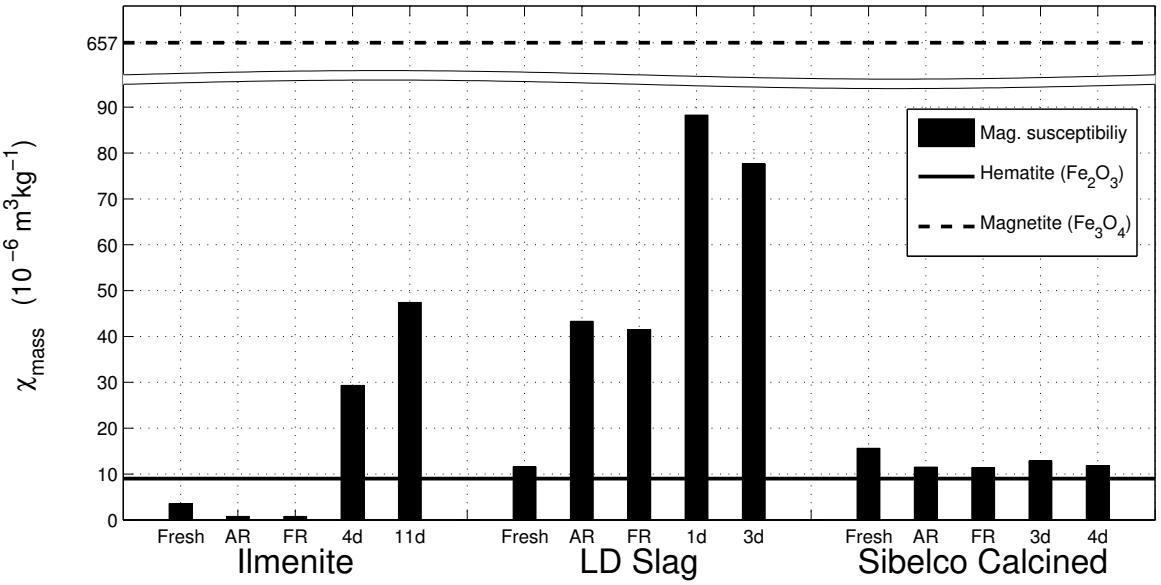

Figure 5.1: Mass specific magnetic susceptibility for three different oxygen carrier materials. For each material there is an unused sample that has not been used in a combustor, and two samples taken from the air and fuel reactor (AR and FR) in a CLC facility, and samples taken after different usage times in an OCAC process.

5.2 Intermediate Summary

In the previous section, the results of the magnetic susceptibility measurements of the pure metal-oxides as well as the investigated oxygen carrier materials have been shown. In Table 5.3 a summary of the conclusions drawn in this section are given, along with some questions that will need to be answered.

Table 5.3: Intermediate summary of magnetic susceptibility measurements.

	Conclusion/Question	Explanation
C1	Magnetite (Fe_3O_4) has the highest magnetic susceptibility of the measured pure oxide phases.	
C2	The magnetic susceptibility of LD Slag and ilmenite varies depending on usage, while Sibelco Calcined has relatively stable susceptibility.	
Q1	Do all oxygen carriers with a susceptibility above 9×10^{-6} m^3kg^{-1} contain magnetite?	Section 5.3
Q2	Why does LD Slag have higher susceptbilitiy than ilmenite?	Section 6.3.3
Q3	Does the magnetic susceptibility data correlate to data of magnetic fraction?	Section 6.1

5.3 Phase Analysis Using XRD

A first thing to mention concerning the XRD results is that some of the resulting diffractograms contained a lot of noise and thus they were difficult to evaluate (as shown in Figure 4.2). This is a somewhat expected outcome as it is not pure substances that are being analyzed, but rather a myriad of different elements and compositions. Hence, the identified phases have a somewhat high underlying uncertainty.

Table 5.4 shows the results from the XRD analysis. The presented phases are mainly the different metal-oxides that have been considered in this project. In addition to these, many other phases were also found (particularly for LD Slag) for which no further investigation and/or measurements have been made.

First we have ilmenite. Of the different oxygen carriers, these resulted in the clearest diffractograms. As expected, the XRD analysis shows that fresh ilmenite consists of $\mathrm{FeTiO_3}$ as well as hematite ($\mathrm{Fe_2O_3}$). As described in Chapter 3, $\mathrm{FeTiO_3}$ is the reduced phase of the oxygen carrier "ilmenite", which is the state of the received material. For the two CLC samples, both the reduced and oxidized form ($\mathrm{Fe_2TiO_5}$) of the oxygen carrier was found. In the diffractograms, these had very similar patterns (overlapping to a large extent) which could indicate that the sample mostly contains one of them. Since these CLC samples were taken in an oxidized state, $\mathrm{Fe_2TiO_5}$ is the more probable candidate. However, in a well mixed fluidized bed with high circulation rates, it may not be so strange if both reduced and oxidized phases were found in the sample.

Both magnetite and hematite are found in all of the ilmenite-samples taken from the CLC and OCAC process. Both of them were identified as major phases in the OCAC samples and merely as traces in the CLC samples. Why this is will be discussed in Section 6.3.1.

The diffractograms of LD Slag were much less clear and therefore more difficult to analyze and errors may be more prominent. The phases shown in Table 5.4 are the metal-based phases relevant to this work and thus leave out a big portion of the finding for LD Slag. Some of the detected minor- and trace phases were virtually impossible to separate from the background noise. Here hematite seemed to be more abundant in the OCAC samples, while magnetite was more abundant in the CLC samples.

In the XRD analysis of Sibelco Calcined, different manganese oxide phases were found. Fresh, unused Sibelco Calcined contained MnO and $\mathrm{Mn_3O_4}$ which are both some of the more reduced phases of manganese. In the used samples, MnO became less frequent and $\mathrm{Mn_2O_3}$ and $\mathrm{MnO_2}$ (the more oxidized phases) became more noticeable.

Table 5.4: Detected metal-based phases from XRD analysis The table shows major, minor and trace phases, which denotes presence in a sample in decreasing order. In the header for OCAC, time in the combustor is shown in days for ilmenite/LD Slag/Sibelco Calcined.

		Fresh	CLC		OCAC	
			AR	FR	4/1/3d	11/2/4d
Ilmenite	Major	$FeTiO_3$	$FeTiO_3$[(1)] Fe_2TiO_5[(1)]	$FeTiO_3$[(2)] Fe_2TiO_5[(2)]	Fe_2O_3 Fe_3O_4	Fe_2O_3 Fe_3O_4
	Minor	Fe_2O_3	TiO_2		Fe_2TiO_5 TiO_2	TiO_2
	Trace		Fe_2O_3 Fe_3O_4	Fe_2O_3 Fe_3O_4	$FeTiO_3$	
LD Slag	Major		Fe_3O_4	Fe_3O_4	Fe_2O_3	Fe_2O_3
	Minor	Fe_2O_3	Mn_3O_4	FeO		
Sibelco	Major	MnO, Mn_3O_4	Mn_2O_3, Mn_3O_4	Mn_2O_3, Mn_3O_4	Mn_3O_4	Mn_3O_4
	Minor	Mn_2O_3		MnO	Mn_2O_3	Mn_2O_3

[(1)],[(2)]...Material likely contains one or combination of phases with same superscript

5.4 Intermediate Summary

In Table 5.5, a summary of the conclusions drawn in the XRD analysis is given. A question is also stated, which will be discussed further in the sections indicated in the table.

Table 5.5: Intermediate summary of XRD analysis.

	Conclusion/Question	Explanation
C1	Not all samples with a susceptibility over 9×10^{-6} m^3kg^{-1} contain magnetite. Neither does Sibelco Calcined or all LD Slag samples seem to have magnetite present.	
C2	The diffractograms of LD Slag are difficult to analyze.	
Q1	Why is there no magnetite detected in LD Slag/OCAC and Sibelco Calcined?	Section 6.3.2, Section 6.4

5.5 Elemental Analysis Using SEM–EDX

In this section, a selection of SEM and EDX images is shown. In the Appendix, additional SEM images taken of particles and their surfaces are found. The majority of the EDX images acquired show single particles, this is however a slight drawback as the different particles in a sample can have very different compositions. In Figure 5.2 a SEM image of multiple fresh LD Slag particles is shown. This shows, in addition to a varying composition, that the particles also have varying form and size.

The obtained SEM images of the three oxygen carrier materials also give information about the topography of the particles. A find that was consistent for all of the three oxygen carriers is that the fresh sample of each batch has a smooth surface while the samples that had been used in a CLC or an OCAC process has a porous surface. This difference is demonstrated for ilmenite in Figure 5.3, where images have been taken at the same magnification. Close-up images of a particle from each sample are found in Figures A.3, A.4 and A.5 in the Appendix.

In Figure 5.4, three EDX maps are shown for fresh Sibelco Calcined, with manganese to the left, iron in the middle and oxygen to the right. This gives an indication of the relative concentration of each element near the surface, showing that manganese and oxygen are more abundant than iron for this Sibelco Calcined particle. This is in agreement with the elemental composition information that was given in Table 3.3 in Chapter 3.

EDX maps were also made of a polished LD Slag particle in search after potential migration of iron, which has been reported is the case of ilmenite. EDX analysis showed no

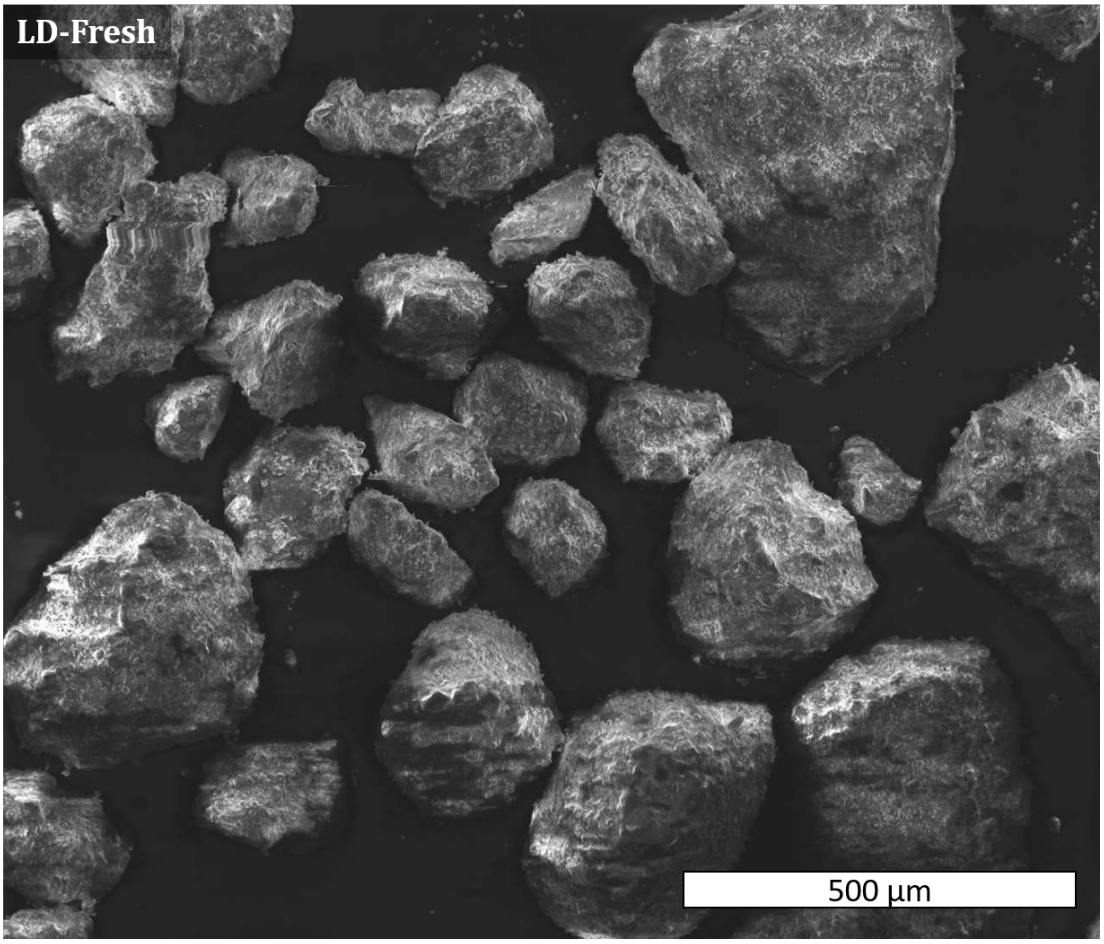

Figure 5.2: SEM image of multiple fresh LD Slag particles.

evidence of iron migration to the surface, as can be seen in Figure 5.5. This figure also shows that calcium, on the other hand, seems to migrate to the surface, leaving a silicon dense core. This is however not something that would affect the magnetic properties by the knowledge acquired in this work. All of the EDX maps of this particle are shown in Figure A.2.

It should again be noted that EDX maps were only made on a single LD Slag particle. Since LD Slag can be rather heterogeneous, a different particle may look different.

In Figure 5.6, EDX maps are displayed for the iron and titanium distribution of fresh ilmenite and ilmenite that have been used in CLC and OCAC operation. From this, we can see that the iron and titanium content is about the same for the fresh ilmenite particle, which is in agreement with the XRD results which showed that fresh ilmenite mainly contains $FeTiO_3$ (thus an equal quantity of iron and titanium). In Figure 5.6 we also see that there is more abundance of titanium than of iron in both the CLC and the OCAC samples. But the iron content seems to be the lowest for the CLC sample. This will be revisited in Section 6.3.1 in the discussion of the possible erosion of the surface of ilmenite particles.

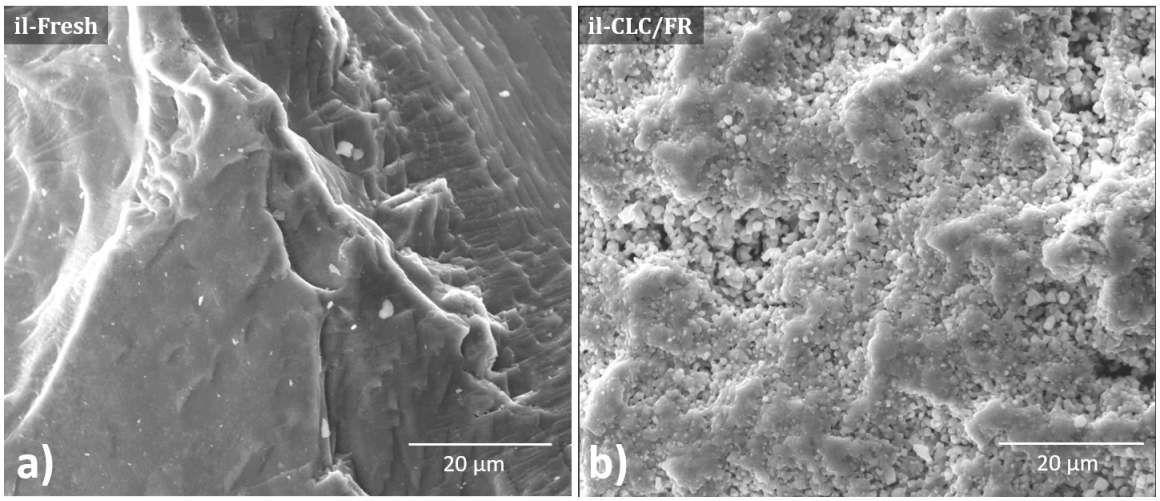

Figure 5.3: SEM images demonstrating the difference in topography of ilmneite. a) shows the surface of a fresh ilmenite particle and b) shows the surface of a particle that has been used in CLC.

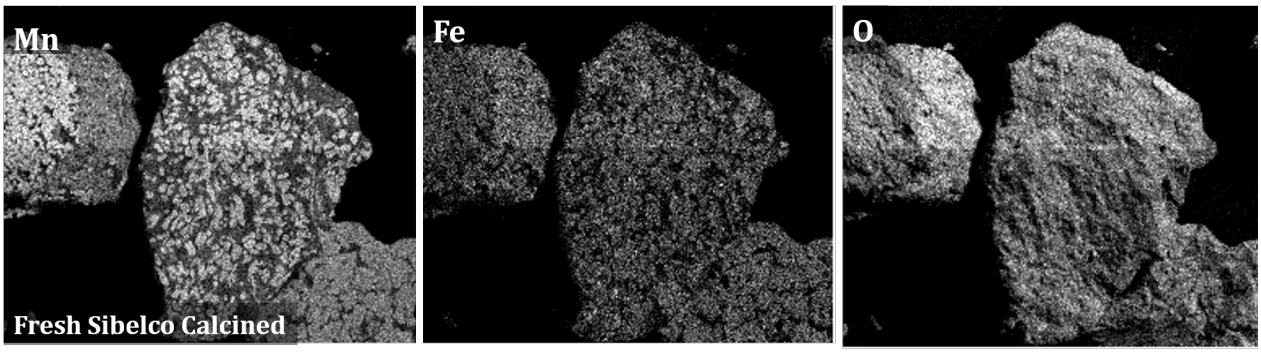

Figure 5.4: EDX maps of a fresh Sibelco Calcined particle, showing the distribution of manganese to the left, followed by iron and oxygen to the right.

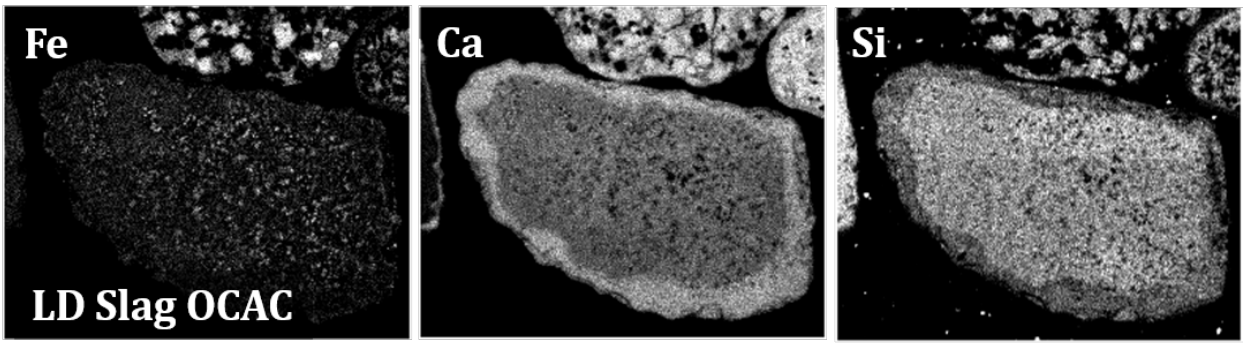

Figure 5.5: EDX maps of the cross-section of a LD Slag particle that has been in a OCAC process. The distribution of iron is shown to the left, following by calcium and silicon to the right.

5.6 Intermediate Summary

In Table 5.6, a summary of the main conclusions of the SEM–EDX analysis is shown.

Table 5.6: Intermediate summary for the SEM-EDX analysis

	Conclusion
C1	All fresh oxygen carriers investigated have smooth surfaces.
C2	All used samples investigated have porous surfaces.
C3	No indication for migration of iron to the surface was detected for LD Slag.

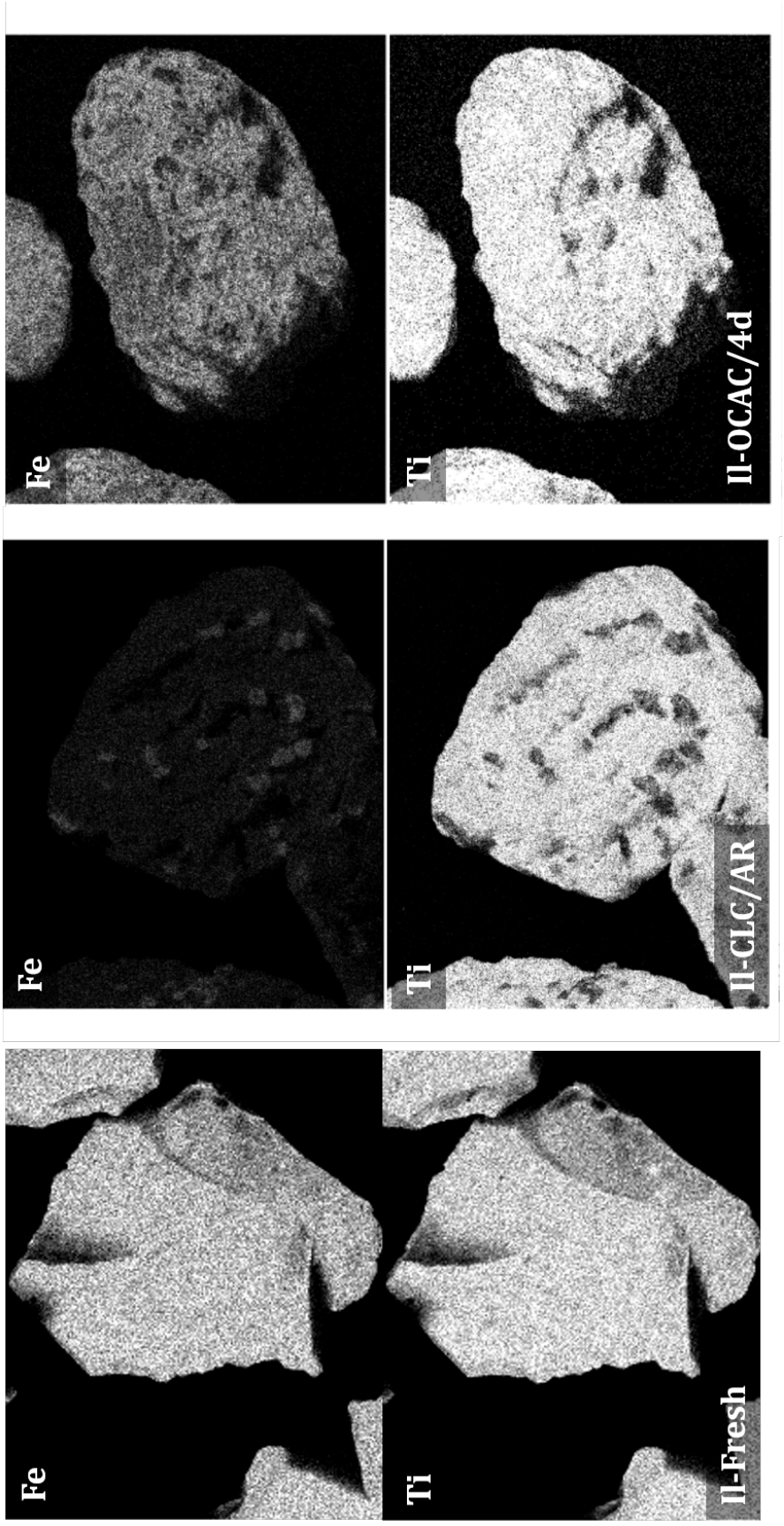

Figure 5.6: EDX maps for iron and titanium distribution for three ilmenite samples.

Chapter 6

Analysis and Discussion

In this chapter, a more extensive interpretation is made of the results presented in the previous chapter. This will partly be made through comparisons between the different samples of oxygen carriers that have been measured. The questions that were stated at the end of each section in Chapter 5 will be answered to the extent possible. This chapter ends with an investigation of the possible sources of error that could affect the accuracy of the results.

6.1 Correlation Between Susceptibility and Magnetic Fraction

One of the aims of this work was to find whether there is a correlation between measurements of magnetic susceptibility and the magnetic fraction, previously recorded. We therefore begin the discussion by putting the obtained results of magnetic susceptibility in comparison to the data of magnetic separability obtained by Andersson et al. This is shown in Figure 6.1 where susceptibility is shown in black bars to the left and magnetic fraction shown in white to the right. From this, we see that there are similarities in the trends, but also that there is no one-to-one correlation between susceptibility and magnetic fraction.

In Figure 6.2 we see magnetic susceptibility and separability plotted against each other. In this graph, we do not look explicitly at which facility they have been used in. This shows more clearly that there seems to be a linear dependency between the two measures of magnetism. Sibelco Calcined – which has been noted being more stable in its magnetic properties – shows a clearly linear behaviour, while the data points of the other two materials deviate more from their fitted lines which indicates that a linear correlation does not represent the measurements perfectly.

This more linear behavior of Sibelco Calcined suggests that, for this oxygen carrier, the magnetic fraction could be estimated from a simple magnetic susceptibility measurement with higher certainty than for the other two iron-based oxygen carriers. This would make the research of magnetic separation (where data of this kind is needed) easier as this would mean that tedious tests of magnetic fraction using a bulky band feeder would not be necessary. It is however also important to note that the fitted lines are created

with few data points, so the accuracy of such an estimation would be questionable.

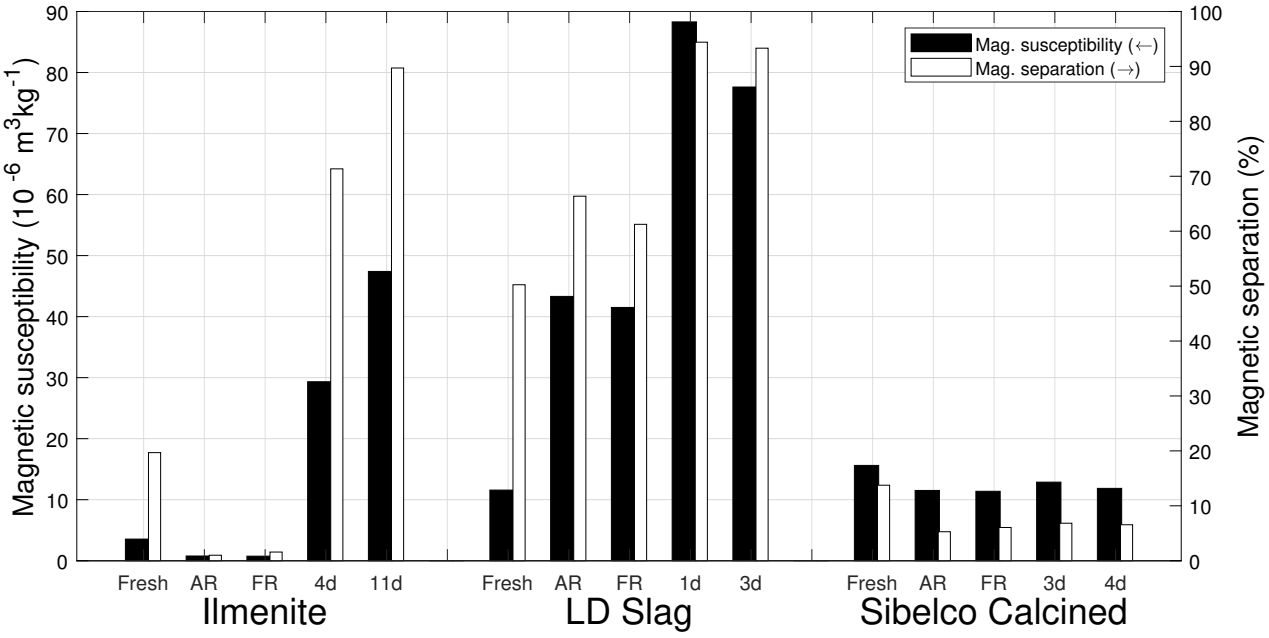

Figure 6.1: Comparison of magnetic susceptibility and magnetic separation degree. The former is shown in black bars to the left and the latter in white bars to the right.

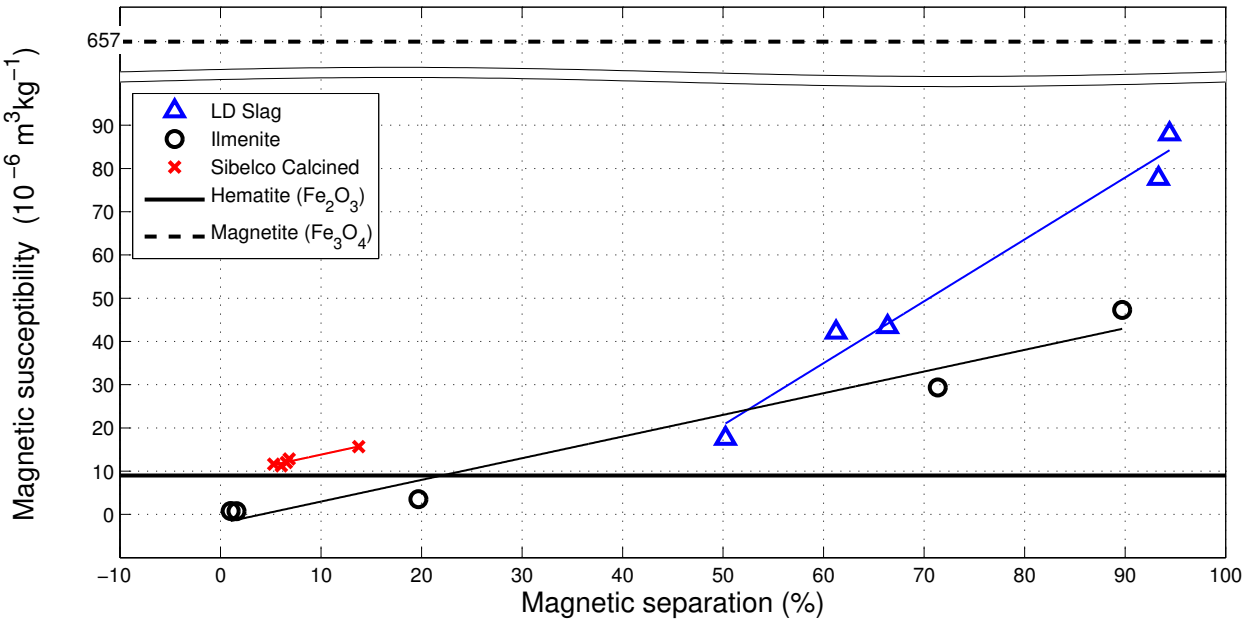

Figure 6.2: Magnetic susceptibility plotted against magnetic separation.

6.2 The Significance of Magnetite

One of the first finds in this work was the indication that the amount of magnetite in a material is imperative to the magnetic susceptibility of the oxygen carriers. To clarify to what degree this seems to be confirmed, the predicted presence of magnetite in the different oxygen carrier materials made in Section 5.1 in comparison to the actual finds of magnetite from the XRD analysis are shown in Table 6.1.

In this, we can see that there are inconsistencies, especially for LD Slag and Sibelco Calcined. In the cases where disagreements are found, explanations will be offered in the sections indicated in Table 6.1

Table 6.1: Comparison of predicted presence of magnetite to XRD analysis. 'X' denotes strong predictions or major phases found, and 'o' denotes less strong predictions or minor phases found.

Oxygen carrier	Predicted presence of magnetite†	Magnetite found in XRD‡	Agreement	Explanation
il-Fresh	–	–	Yes	Section 6.3.1
il-CLC/AR	–	o/–	No/Yes	
il-CLC/FR	–	o/–	No/Yes	
il-OCAC/4d	X	X	Yes	
il-OCAC/11d	X	X	Yes	
LD-Fresh	X	–	No	Section 6.3.2
LD-CLC/AR	X	X	Yes	
LD-CLC/FR	X	X	Yes	
LD-OCAC/1d	X	–	No	
LD-OCAC/1d	X	–	No	
SIB-Fresh	o	–	No	Section 6.4
SIB-CLC/AR	o	–	No	
SIB-CLC/FR	o	–	No	
SIB-OCAC/3d	o	–	No	
SIB-OCAC/4d	o	–	No	

†...In accordance to measured χ_{mass} of metal-oxides in Section 5.1
‡...See Table 5.4

6.3 Comparing Fe-based Oxygen Carriers

In this section, comparisons will be made of different samples within and between the two groups of Fe-based oxygen carriers. No distinction between the CLC and the OCAC

samples for each oxygen carrier material will be made. After the differences are reviewed for each comparison, explanations (to the extent possible) are given.

6.3.1 Ilmenite

6.3.1.1 Fresh – OCAC

Compared to the fresh sample, both magnetic fraction and susceptibility increased after use in the OCAC process (as can be seen in Figure 6.1). XRD analysis shows that fresh ilmenite mostly contains $FeTiO_3$ and some hematite, while ilmenite used in the OCAC process contains an abundance of hematite as well as magnetite; the two most magnetic phases measured in this work. The surfaces of the fresh ilmenite particles are smooth, while used ilmenite has a slightly porous topography.

The possible reasons for ilmenites increased magnetic behaviour are twofold:

1. Fresh ilmenite was received in a reduced state (as confirmed by the XRD results), while used ilmenite had undergone oxidation. Of the different oxidation phases for iron, the two more oxidized ones are rather magnetic. The reduced state of ilmenite ($FeTiO_3$), on the other hand, has lower magnetic susceptibility than both magnetite and hematite, as can be seen in the table of magnetic susceptibility, Table A.1. Thus, ilmenite would become more magnetic.

2. As described in Section 3.1.1, iron migrates to the surface of ilmenite particles during repeated redox cycles thus increasing the local iron concentration and allowing for further formation of pure iron-oxides, which have a high magnetic susceptibility.

The change in topography seen in the SEM-images is not assumed to affect the magnetic properties of the material. Reports have been made on increasing reaction rates due to the larger reaction surface[34], but no suggestions have been seen of this affecting magnetism.

6.3.1.2 Fresh – CLC

After use in chemical-looping combustion, both the magnetic fraction and the magnetic susceptibility decreased (though susceptibility to a greater extent). The XRD results show that while both fresh ilmenite and ilmenite samples that have been used in CLC process contain $FeTiO_3$, the latter contains far less hematite (both magnetite and hematite were found as trace phases which could be part of the background noise). SEM-images show that the particles from the samples used in the CLC process have a more porous surface, compared to those from the OCAC process.

A decrease in the already low hematite concentration explains the relative decrease in magnetic behaviour. Previous studies have found that iron migration occurs in both

CLC- and OCAC operations[9, 23, 35].

The iron migration process which increased the magnetic behaviour of ilmenite used in the OCAC process, might be the reason why it has decreased for ilmenite used in the CLC process: The increased porosity of the particles decreases the particles' crushing strength. This might furthermore lead to that the outer, iron-rich layer becomes broken down and lost as fly ash in the flue gas. This was considered by Cuadrat et al.[24] who observed the increased porosity in ilmenite particles and suggested that only the iron-rich outer layer would be broken down. Andersson et al. who conducted a preceding study of this work found that the ilmenite particles used in CLC had decreased in size. The tougher treatment in CLC conditions (due to higher temperatures, reduction speed and deeper reduction) also creates stresses on the lattice structure of the particles.

It was also seen in Figure 5.6 that the relative iron content seems to be lower in the CLC samples than in the OCAC samples (based on the particular particles studied), which further strengthens the suggestion that the iron-rich layer becomes somewhat eroded.

6.3.2 LD Slag

6.3.2.1 Fresh – OCAC

As for ilmenite, the magnetic properties increased after use in OCAC. Though the XRD analysis was difficult to make, an increase of hematite was noticed. The SEM-images shows, similar to the ilmenite particles, that the surface becomes slightly more porous.

Though LD Slag does not undergo iron migration as was discussed in Section 5.5 and can be seen in Figure A.2, the used sample is expected to be more oxidized (and thus more magnetic) than the fresh sample which seems to be the case by looking at the XRD results.

6.3.2.2 Fresh – CLC

LD Slag used in chemical-looping combustion does not suffer the same decrease in magnetic properties as ilmenite, as seen in Table 5.2. But as with ilmenite, LD Slag samples that have been used in the CLC process have lower magnetic properties than that which have been used in the OCAC process. XRD analysis shows the highly magnetic magnetite (Fe_3O_4) as a major phase for the CLC samples.

LD Slag does not undergo the process of iron migration, which suggests that LD Slag is able to retains large amounts of its iron after use in chemical-looping, despite undergoes erosion of its surface. Thus preserving its ability to create more magnetic iron-oxides.

6.3.3 Why is LD Slag More Magnetic Than Ilmenite?

Finally, we will look at the difference between the two iron-based oxygen carries, especially at the samples used in the OCAC process. By the conclusions drawn at the beginning of Section 5.1 about the magnetism concerning the pure metal-oxides, ilmenite samples would be expected to have a higher magnetic susceptibility than LD Slag samples because:

- Ilmenite contains more magnetite than LD Slag (see Table 5.4).
- Ilmenite contains more iron than LD Slag (37 vs. 14 mass%, see Table 3.3), which would increase chance of formation of pure iron-oxides.

All this, however, is contradicted by the susceptibility results in Table 5.2, as well as the magnetic fraction measured by Andersson et al. (though not to the same extent), where the ilmenite samples have a lower magnetic susceptibility than LD Slag.

In an attempt to explain this inconsistency, the low-quality diffractograms of LD Slag can be blamed. Due to the difficulty in analyzing this oxygen carrier, there might be amounts of magnetite in LD Slag that has been mis-identified as something else. The fact that the samples total magnetic susceptibility is higher than hematite also supports the existence of magnetite.

Another possibility is that some of the other compositions formed in LD Slag exhibit very high susceptibility. But as this has not been studied in this work, no conclusion of that sort can be made.

6.4 Comparing Mn-based to Fe-based Oxygen Carriers

As was seen in Table 5.2, Sibelco Calcined had an overall lower magnetic susceptibility and magnetic fraction than the other oxygen carrier materials. The reason for this has already been suggested in the previous chapter: None of manganese's oxidation states are particularly magnetic, at least not in comparison to the oxidation states of iron. This is also the reason for Sibelco Calcined's relative stable magnetic behaviour between use in different processes.

It was also seen that the magnetic susceptibility measurements (Table 5.2) of Sibelco Calcined were higher than the individual manganese oxides and even higher than what was measured for hematite. It could therefore be suggested that all of the Sibelco Calcined samples contain small amounts of magnetite, which is conceivable as Sibelco Calcined indeed does contain some amounts of iron, see Table 3.3. Using Equation (2.3) puts the estimated concentration of magnetite to about 2 mass%.

There exist many different types of manganese ores. A suggestion can therefore be to use manganese ores with high concentration of iron in order to increase the magnetic properties of a manganese-based oxygen carrier.

6.5 Sources of Error

In this section, some sources that could have led to errors are stated. Starting with the measurements of the magnetic susceptibility of the metal-oxides. As was commented on in Section 5.1, these particles are much finer than the particles in the sample group. This could have an effect on the magnetic susceptibility. These metal-oxides were, however, not found anywhere in a suitable size-range. Despite this, the measurements made on these demonstrated the difference between the different phases.

Another source of error is the quantity in which the different oxygen carriers were received, which was approximately 200 ml for each oxygen carrier. If this is a good representation of the original batch is not known. Further was only a small amount of this used in the XRD analysis and a yet smaller amount for the SEM-EDX analysis. For the case of EDX analysis, measurements were only made on single particles for each sample. This amounts to that conclusions might have been drawn for the entire sample that did not represent the whole. It was, nonetheless, assumed that this would give an adequate representation of the whole.

Chapter 7

Conclusion

In this master's thesis, the magnetic behaviour of three oxygen carrier materials, which have been used in either CLC- or OCAC operation, have been investigated. This was done with the ambition to obtain a better understanding of the mechanisms that govern the materials' magnetic properties. An ambition was also to search for correlations to the materials' magnetic fraction, which were measured in a proceeding project. The investigation has been carried out through elemental analysis using SEM-EDX, phase analysis using XRD and measurements of the samples' magnetic susceptibility.

Investigation of various manganese- and iron-oxides – which are possible phases in the studied oxygen carrier materials – showed that magnetite has significantly higher magnetic susceptibility than the other measured phases. The importance of magnetite for highly magnetic materials was further supported by the XRD analysis, which indicated that many samples with a high magnetic susceptibility also contained magnetite.

The measurements of the different oxygen carrier materials' magnetic susceptibility had similarities to the previous measurements of magnetic separability. The manganese-based oxygen carrier, Sibelco Calcined, had the strongest correlation between magnetic susceptibility and magnetic separability. The magnetic behaviour of this oxygen carrier material was similar for all samples, regardless of what combustion process (i.e. CLC or OCAC) the samples came from. The magnetic susceptibility and magnetic separability of the two iron-based oxygen carriers, ilmenite and LD Slag, did not correlate to the same extent as for Sibelco Calcined. The magnetic behaviour of ilmenite and LD Slag varied substantially depending on whether the samples had been used in CLC- or OCAC operation.

Due to insufficient correlation, a model that would predict the magnetic fraction of oxygen carrier materials, could not be established. Neither can the change in magnetic behaviour of an oxygen carrier material, post-combustion, be predicted. Rough trends may, however, be laid out that estimate whether the magnetic behaviour will increase, decrease or remain the same after use in combustion operation.

From what has been found in this work, iron-based oxygen carriers seem to be more favourable for magnetic separation of used bed materials. Strong indications have been made that oxygen carriers forming the iron-oxide magnetite at the time of extraction is desired in this context. For manganese-based oxygen carrier materials, suggestions can be made to use manganese ores with high concentrations of iron, as this can increase

the magnetic properties of the oxygen carrier.

Bibliography

[1] E. A. Mathez and J. E. Smerdon, *Climate Change – The Science of Global Warming and Our Energy Future* (Columbia University Press, 2018).

[2] M. P. S. Ute Kehse, *Global warming doesn't stop when the emissions stop*, https://phys.org/news/2017-10-global-doesnt-emissions.html (visited on 05/24/2019).

[3] T. L. Frölisher, M. Winton and J. L. Sarmiento, "Continued global warming after CO_2 emissions stoppage", Nature Climate Change **4**, 40–44 (2014).

[4] UNFCCC, *The paris agreement*, https://unfccc.int/process-and-meetings/the-paris-agreement/the-paris-agreement (visited on 02/07/2019).

[5] M. Rydén, A Lyngfelt, Ø. Langørgen et al., "Negative CO_2 Emissions with Chemical-Looping Combustion of Biomass – a Nordic Energy Research Flagship Project", Energy Procedia **114**, 6074–6082 (2017).

[6] J. Koornneef, M. Junginger and A. Faaij, "Development of fluidized bed combustion –An overview of trends, performance and cost", Progress in Energy and Combustion Science **33**, 19–55 (2007).

[7] H. Thunman, F. Lind, C. Breitholtz et al., "Using an oxygen-carrier as bed material for combustion of biomass in a 12-MW_{th} circulating fluidized-bed boiler", Fuel **113**, 300–309 (2013).

[8] M. Rydén, M. Hanning and F. Lind, "Oxygen Carrier Aided Combustion (OCAC) of Wood Chips in a 12 MW_{th} Circulating Fluidized Bed Boiler Using Steel Converter Slag as Bed Material", Applied Sciences **8**, 2657 (2018).

[9] P. Moldenhauer, M. Rydén, A. Lyngfelt, "Testing of minerals and industrial by-products as oxygen carriers for chemical-looping combustion in a circulating fluidized-bed 300 W laboratory reactor", Fuel **93**, 351–363 (2012).

[10] A. Lyngfelt and C. Linderholm, "Chemical-Looping Combustion of Solid Fuels – status and recent progress", Energy Procedia **114**, 371–386 (2017).

[11] W. K. Lewis, E. R. Gilliland, and G. T. McBride, "Gasification of Carbon by Carbon Dioxide in Fluidized Powder Bed", Industrial & Engineering Chemistry **41 (6)**, 1213–1226 (1949).

[12] T. Mattisson, M. Keller, C. Linderholm et al., "Chemical-looping technologies using circulating fluidized bed systems: Status of development", Fuel Processing Technology **172**, 1–12 (2018).

[13] A. Lyngfelt, B. Leckner and T. Mattisson, "A fluidized-bed combustion process with inherent CO_2 separation; application of chemical-looping combustion", Chemical Engineering Science **56**, 3101–3113 (2001).

[14] P. Wang, H. Leion and H. Yang, "Oxygen-Carrier-Aided Combustion in a Bench-Scale Fluidized Bed", Energy Fuels **31**, 6463–6471 (2017).

[15] M. Källén, M. Rydén and F. Lind, "Improved Performance in Fluidised Bed Combustion by the Use of Manganese Ore as Active Bed Material", 22nd International Conference on Fluidized Bed Conversion, 14-17 June 2015, Turku (2015).

[16] C. Kittel, *Introduction to Solid State Physics (Eighth edition)* (Wiley, 2005).

[17] B. D. Cullity and C. D. Graham, *Introduction to Magnetic Materials, Second Edition* (IEEE Press, 2009).

[18] John A. Dearing, *Environmental Magnetic Susceptibility – Using the Bartington MS2 System* (Bartington Instruments, 1999).

[19] Elin Andersson, Mimmi Engvall, Rasmus Erlandsson et al., "Magnetisk separation av bäddmaterial för CO_2 negativ el- och värmeproduktion", MA thesis (Chalmers University of Technology, 2018).

[20] B. Santos, E. Loginova, A. Mascaraque et al, "Structure and magnetism in ultrathin iron oxides characterized by low energy electron microscopy", Journal of Physics: Condensed Matter **21**, 314011 (2009).

[21] H. M. King, *Pictures of igneous rocks*, `https://geology.com/rocks/igneous-rocks.shtml`.

[22] J. Steenkamp, P. Pistorius, and N. Allen, "Reflections on ilmenite roasting and magnetic separation", in, Vol. 2005 (Nov. 2005), pp. 133–141.

[23] Adánez, Juan and Cuadrat, Ana and Abad, Alberto and Gayán, Pilar and de Diego, Luis F. and García-Labiano, Francisco, "Ilmenite Activation during Consecutive Redox Cycles in Chemical-Looping Combustion", Energy & Fuels **24**, 1402–1413 (2010).

[24] A. Cuadrat, A. Abad, J. Adánez et al., "Behavior of ilmenite as oxygen carrier in chemical-looping combustion", Fuel Processing Technology **94**, 101–112 (2012).

[25] Angelica Corcoran, Jelena Marinkovic, Fredrik Lind, Henrik Thunman, Pavleta Knutsson and Martin Seemann, "Ash Properties of Ilmenite Used as Bed Material for Combustion of Biomass in a Circulating Fluidized Bed Boiler", Energy Fuels **25**, 7672–7679 (2014).

[26] B. Das, S. Prakash, P.S.R. Reddy and V.N. Misra, "An overview of utilization of slag and sludgefrom steel industries", Resources, Conservation and Recycling **50**, 40–57 (2007).

[27] J. Adanez, A. Adab, F. Garcia-Labiano et al., "Progress in Chemical-Looping Combustion and Reforming technologies", Progress in Energy and Combustion Science **38**, 215–282 (2012).

[28] Magnus Rydén, Henrik Leion, Tobias Mattisson, Anders Lyngfelt, "Combined oxides as oxygen-carrier material for chemical-looping with oxygen uncoupling", Applied Energy **113**, 1924–1932 (2014).

[29] M. Rydén, M. Hanning and F. Lind, "Improved combustion in fluidized bed with manganese ore as bed material", REPORT 2016:247, Energiforsk AB (2016).

[30] C. Suryanarayana and M. Grant Norton, *X-Ray Diffraction, A Practical Approach* (Springer Science+Business Media, 1998).

[31] Barbara L Dutrow and Christine M. Clark, *X-ray Powder Diffraction (XRD)*, https://serc.carleton.edu/research_education/geochemsheets/techniques/XRD.html (visited on 01/31/2019).

[32] V. Stolojan, *Nanometrology Using the Transmission Electron Microscope* (Morgan & Claypool Publishers, 2015).

[33] Y. Liao, *EDS Acquisition Time*, http://www.globalsino.com/EM/page2517.html (visited on 03/27/2019).

[34] H. Leion, A. Lyngfelt, M. Johansson et al., "The use of ilmenite as an oxygen carrier in chemical-looping combustion", Chemical Engineering Research and Design **86**, 1017–1026 (2008).

[35] P. Moldenhauer, M Rydén, T. Mattisson et al., "The use of ilmenite as oxygen carrier with kerosene in a 300 W CLC laboratory reactor with continuous circulation", Applied Energy **113**, 1846–1854 (2014).

Chapter A

Appendix

A.1 Table of Magnetic Susceptibility for Various Substances

In Table A.1, the magnetic susceptibility of various different minerals are shown.

Table A.1: Different materials and their magnetic susceptibility. Data from published and unpublished sources, showing ranges and individual measurements of susceptibility values and iron content[18].

Mineral/Material	Formula	Iron (mass%)	Mass specific magnetic susceptibility (10^{-6} m^3 Kg^{-1})
Ferromagnetic metals			
Iron	αFe	100	276000
Cobalt	Co	204000	
Nickel	Ni	68850	
Ferrimagnetic			
Magnetite	Fe_3O_4	72	
(0.012-0.069μm)			513-1116
			500-1000
(0.09-2000 μm)			596$\pm$77
(1-250μm)			440-716
			390-580
Maghemite	γFe_2O_3	70	410, 440
			286-371
Titanomagnetite	Fe_3O_4-Fe_2TiO_4		169-290
Titanohaematite	Fe_2O_3-$FeTiO_3$		281-315
Pyrrhotite	Fe_7S_8		50, 53
Greigite	Fe_3S_4		

Table A.2: Continuing of Table A.1

Mineral/Material	Formula	Iron (mass%)	Mass specific magnetic susceptibility (10^{-6} m^3 Kg^{-1})
(Canted) antiferromagnetic			
Hematite	αFe_2O_3	70	1.19-1.69
			0.58-0.78
			0.49-0.65
			0.27, 0.31, 0.6, $<$0.63
Goethite	αFeOOH	63	0.35, 0.38, 0.7, $<$1.26
Paramagnetic (20 °C)			
Ilmenite	$FeTiO_3$	37	1.7, 2
Ulvospinel	Fe_2TiO_4		
Olivine	4[(Mg,Fe)2 SiO_4]	$<$55	0.01-1.3
Siderite	$FeCO_3$	48	1.0
Biotite	Mg,Fe,Al, silicate	31	0.05-0.95
Pyroxene	(Mg,Fe)2Si2O6	$<$12	0.04-0.94
Chamosite	oxidised chlorite		0.9
Nontronite	Fe-rich clay		0.863
Amphibole	Mg,Fe,Al silicate		0.16-0.69
Epidote	Ca,Fe,Al silicate	31	0.25-0.31
Pyrite	FeS_2	47	0.3
Lepidocrocite	γFeOOH	63	0.5-0.75, 0.69
Prochlorite	mica-like mineral		0.157
Vermiculite	complex silicate		0.152
Illite	$K_1Al_4(Si, Al)_8O_2O(OH)_4$		0.15
Bentonite	complex silicate		0.058
Smectite	complex silicate		0.05, 0.027
Chalcopyrite	$CuFeS_2$	30	0.03
Attapulgite	complex silicate		0.02
Dolomite	$CaMg(CO_3)_2$		0.011
Diamagnetic			
Calcite	$CaCO_3$		-0.0048
Alkali-feldspar	Ca,Na,K,Al silicate		-0.005
Plastic			-0.005
Quartz	SiO_2		-0.0058
Organic matter			-0.009
Water	H_2O		-0.009
Halite	NaCl		-0.009
Kaolinite	$Al_4Si_4O_{10}(OH)_8$		-0.019

A.2 SEM–EDX

In Figure A.1, the comparison of two different acquisition times are shown. In Figure A.2, all of the EDX-maps of the cross-section of a LD Slag particle are shown. In Figures A.3, A.4 and A.5, SEM images are shown for a particle from each sample, along with a close-up of the surface.

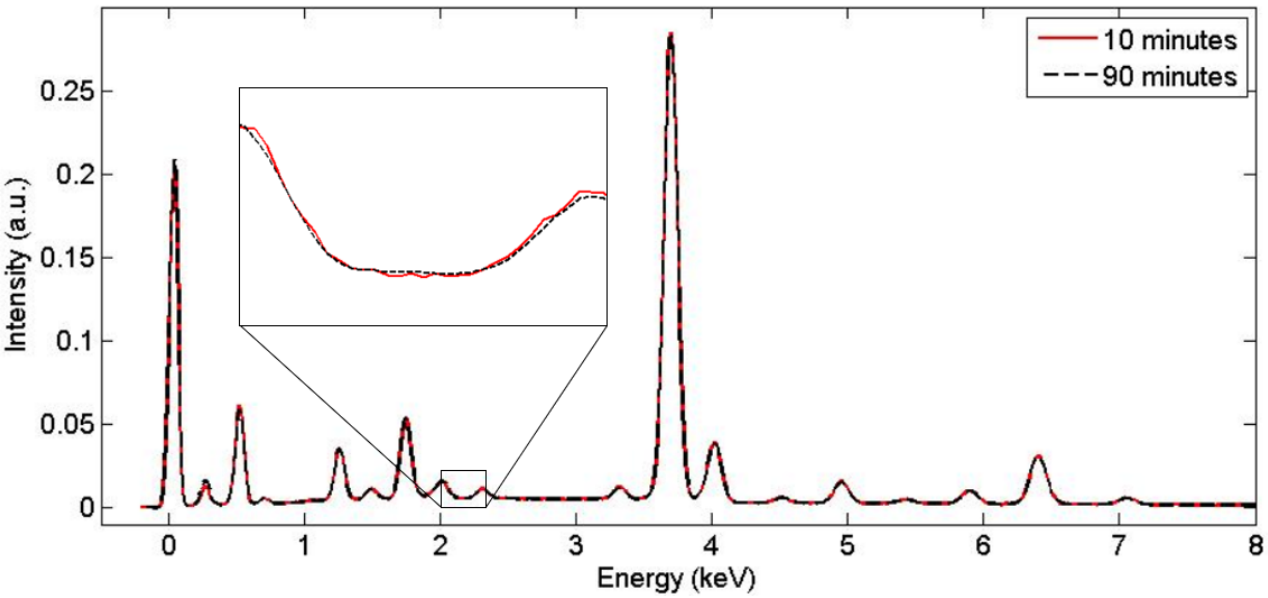

Figure A.1: Normalised SEM–EDX spectra of the same site on LD-OCAC/1d with an acquisition time of 10 minutes and 90 minutes (dashed).

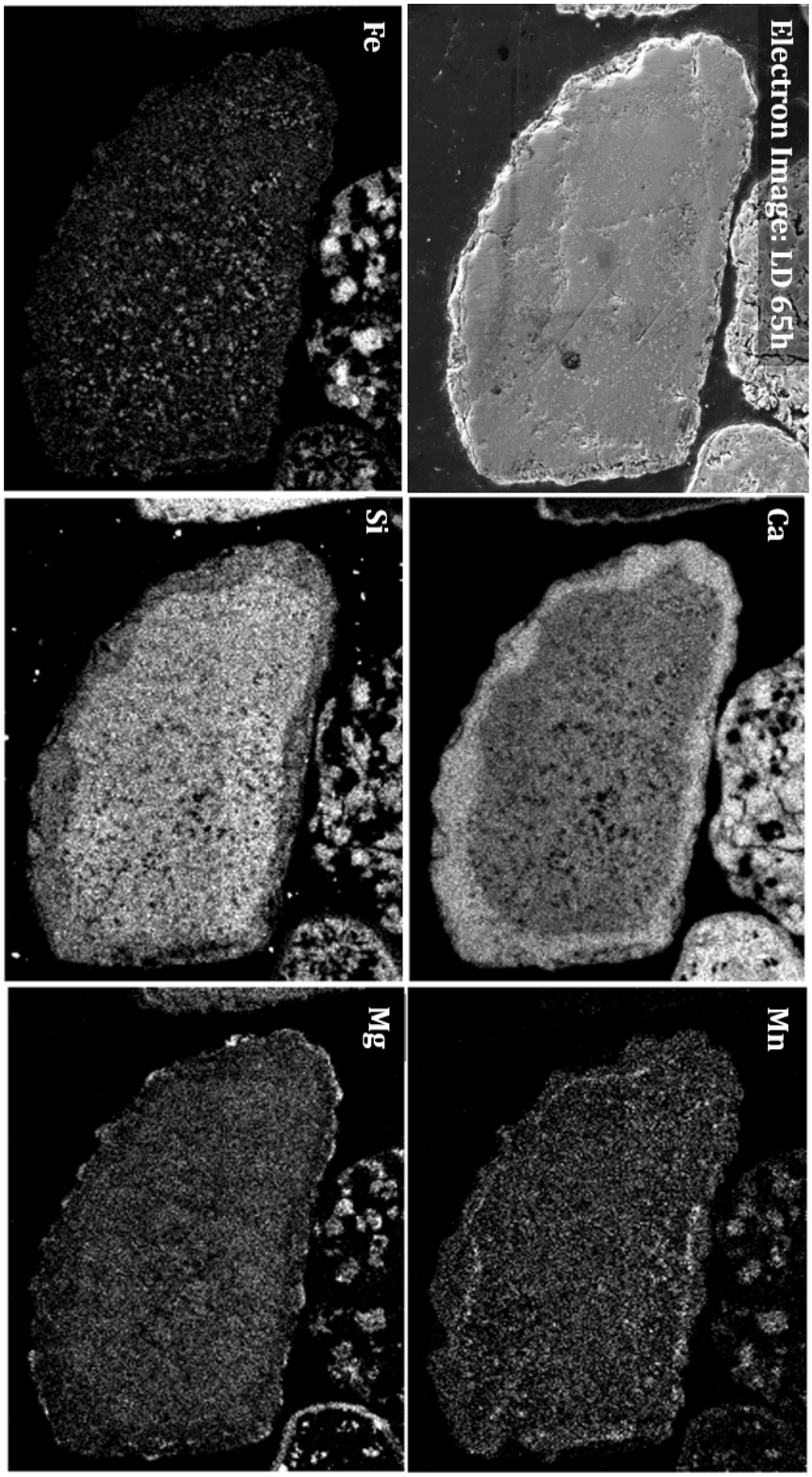

Figure A.2: EDX-map analysis of the cross-section of a LD Slag particle which has been in a OCAC boiler for 65 hours. Maps show Ca are concentrated to the surface as well as some indications of Mn and Mg being more concentrated towards the surface.

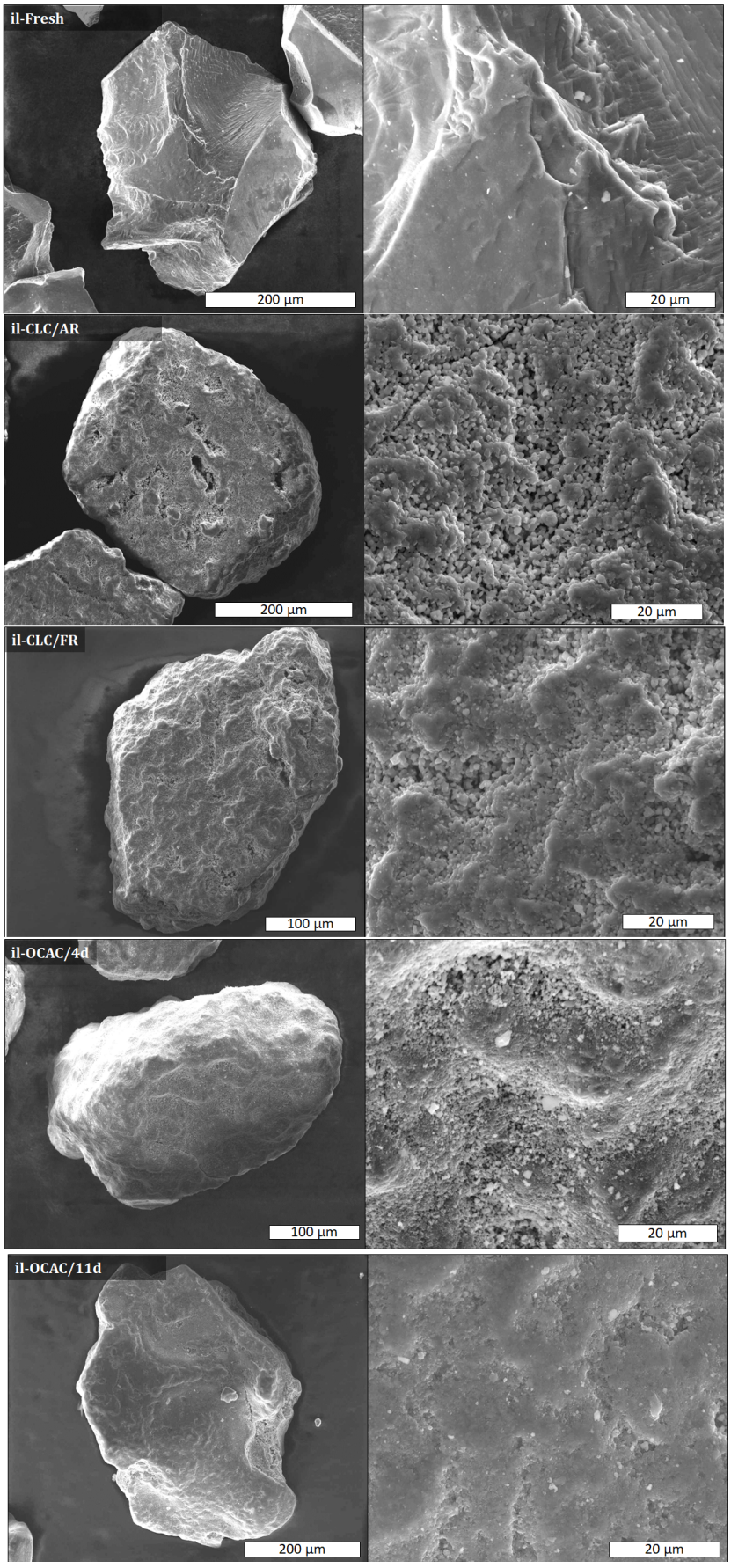

Figure A.3: SEM images of ilmenite particles.

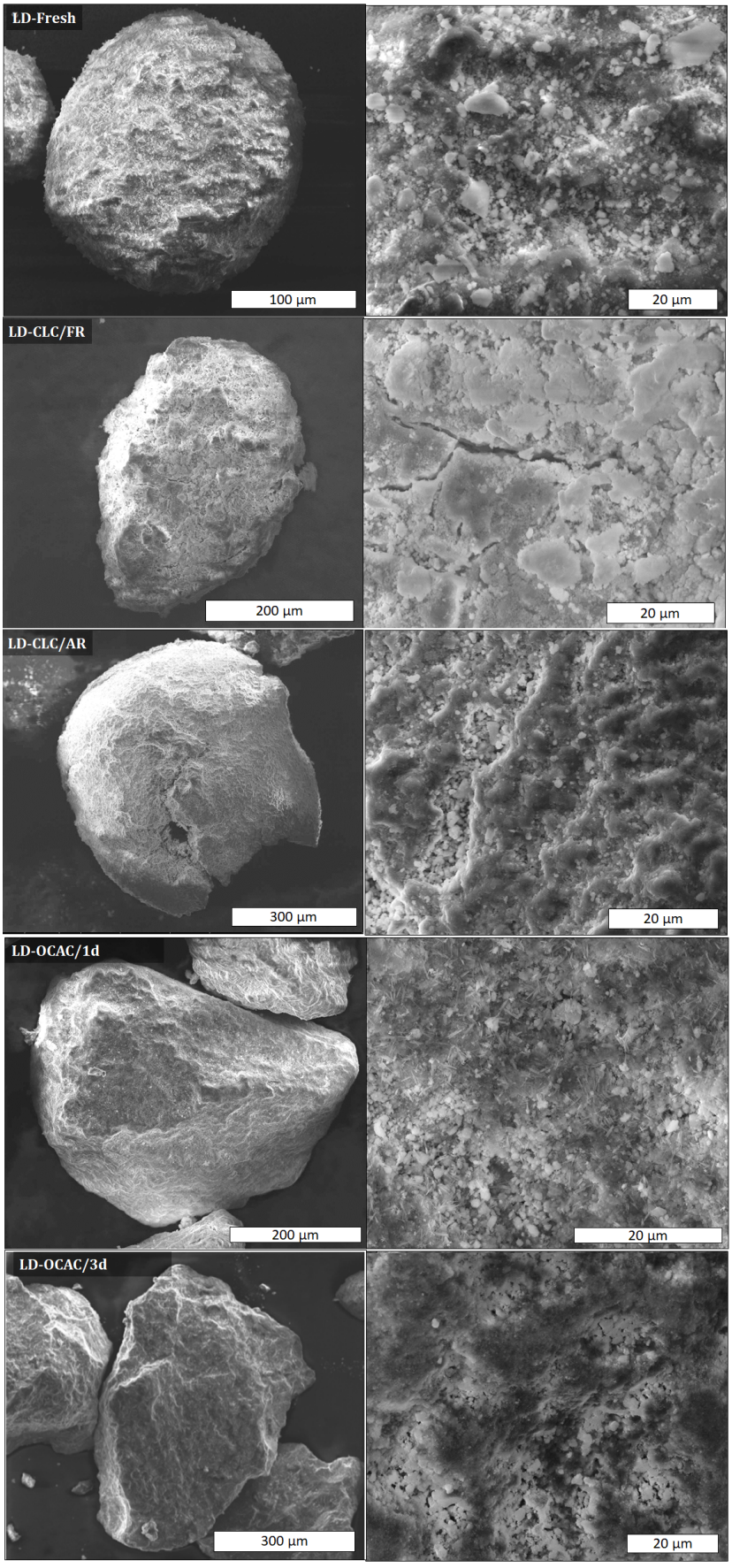

Figure A.4: SEM images of LD Slag particles.

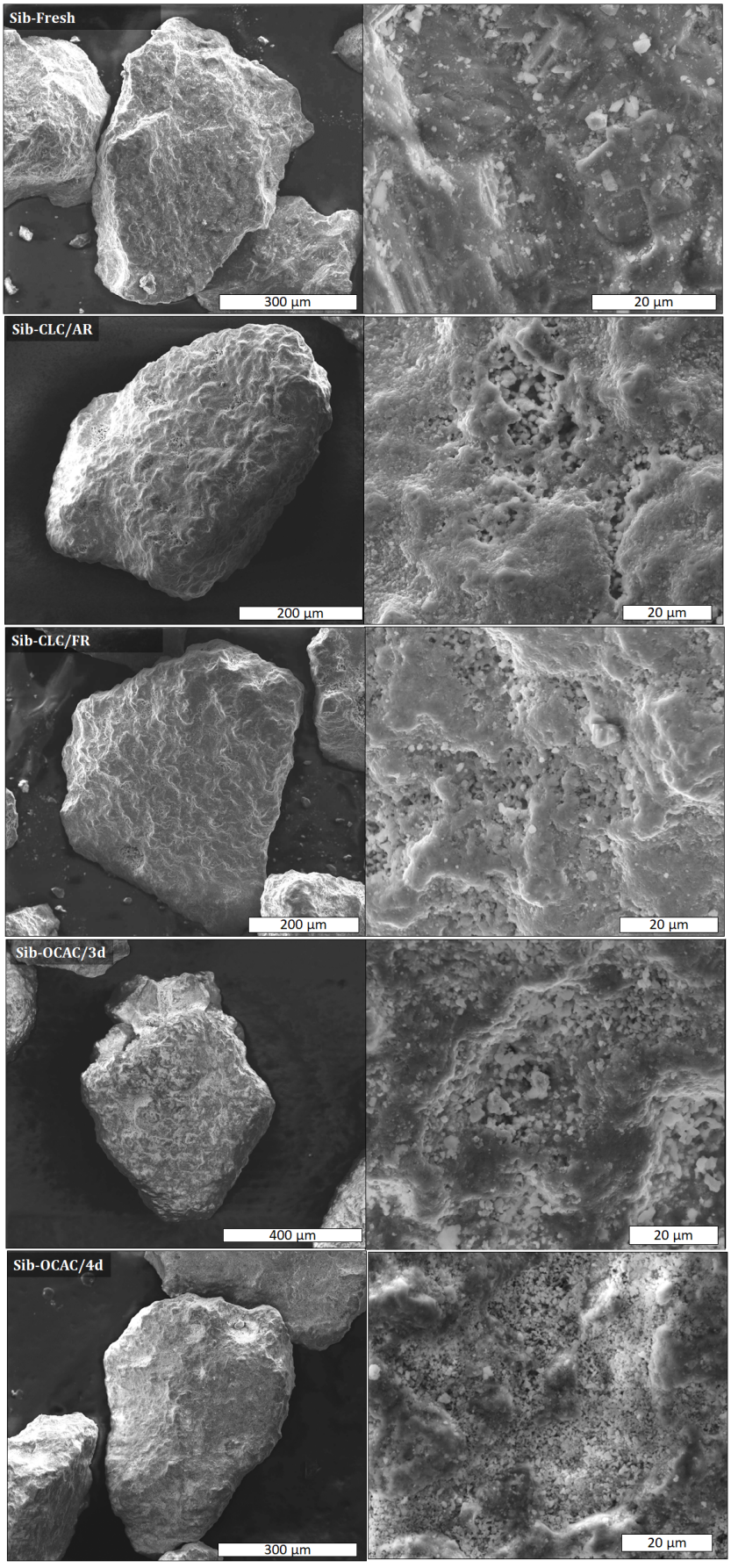

Figure A.5: SEM images of Sibelco Calcined particles.